

# Unifying Decoherence and Phase Evolution in Mixed Quantum–Classical Dynamics through Exact Factorization

Jong-Kwon Ha,<sup>1</sup> Seong Ho Kim,<sup>2</sup> and Seung Kyu Min<sup>2,\*</sup>

<sup>1</sup>*Department of Chemistry, Dalhousie University,  
6274 Coburg Rd, Halifax, NS B3H 4R2, Canada*

<sup>2</sup>*Department of Chemistry, Ulsan National Institute of Science and Technology (UNIST),  
50 UNIST-gil, Ulju-gun, Ulsan 44919, South Korea*

(Dated: November 11, 2025)

We propose new mixed quantum–classical equations of motion within the exact factorization framework to describe electronic coherence and phase evolution simultaneously. The derivation reveals that not only a projected quantum momentum correction, recently identified by Arribas and Maitra [Phys. Rev. Lett. 133, 233201 (2024)], but also a phase-correction appears within the order of  $\hbar$ , providing a unified and rigorous account of electronic coherence and phase evolution as well as their effect on the nuclear force. Benchmark tests on one- and two-dimensional model systems demonstrate that the new formulations capture key nonadiabatic features with high accuracy.

Understanding the coupled motion of electrons and nuclei in molecules remains one of the central challenges in theoretical chemistry and chemical physics. Fully quantum treatments of electron–nuclear dynamics are computationally prohibitive for systems of realistic size, owing to the scaling of the many-body molecular wavefunction. To overcome this limitation, mixed quantum–classical (MQC) methods [1–3] where the electrons are treated quantum mechanically while nuclei follow classical trajectories have become indispensable tools for simulating photochemical processes, charge and energy transfer, and ultrafast dynamics in molecules and materials [4–9]. Among MQC methods, Ehrenfest dynamics [1] and trajectory-based surface hopping [2] are the most widely applied. Despite their utility, they suffer from two fundamental shortcomings: the absence of a reliable mechanism for electronic decoherence, and the lack of a rigorous treatment of phase evolution between adiabatic states. Numerous correction schemes have been proposed, often guided by semiclassical arguments, empirical adjustments, intuition from wave-packet models, or mapping of variables [10–17].

The exact factorization (XF) formalism provides a rigorous foundation for electron–nuclear dynamics by expressing the molecular wavefunction as a product of a nuclear wavefunction and a conditional electronic state [18, 19]. This leads to coupled electronic and nuclear equations of motion that, in principle, include the full electron–nuclear correlation (ENC) effects. XF-based approaches have therefore attracted attention as a systematic framework for deriving improved MQC dynamics [20–31]. In recent work, Arribas and Maitra showed that a projected quantum momentum (PQM) correction naturally arises from the XF formalism and plays a central role in describing electronic coherence [32].

In this work, we derive new mixed quantum–classical equations of motion from the exact factorization formalism, revealing an additional phase-correction term that accompanies the PQM correction of compara-

ble or smaller order in  $\hbar$ . This previously unidentified term governs the proper phase evolution of the Born–Oppenheimer (BO) coefficients. The combined inclusion of PQM and phase corrections provides a balanced and rigorous description of both decoherence and phase dynamics without relying on semiclassical approximations or heuristic arguments, offering deeper conceptual insight into ENC and a practical route to accurate molecular quantum dynamics. We validate the equations through benchmark calculations for the double-arch geometry (DAG) [14] and two-dimensional nonseparable (2DNS) [15] models, which demonstrate that both corrections are essential for reproducing characteristic nonadiabatic features such as Stückelberg oscillations, intermediate-time electronic coherence, and the correct nuclear-density distributions.

The XF formalism expresses the molecular wavefunction  $|\Psi(\underline{\mathbf{R}}, t)\rangle$  as a single product of a time-dependent nuclear wavefunction  $\chi(\underline{\mathbf{R}}, t)$  and an electronic wavefunction  $|\Phi_{\underline{\mathbf{R}}}(t)\rangle$ ,  $|\Psi(\underline{\mathbf{R}}, t)\rangle = \chi(\underline{\mathbf{R}}, t)|\Phi_{\underline{\mathbf{R}}}(t)\rangle$  with partial normalization condition  $\langle\Phi_{\underline{\mathbf{R}}}(t)|\Phi_{\underline{\mathbf{R}}}(t)\rangle_e = 1$  at any  $\underline{\mathbf{R}}$  and  $t$ , where  $\underline{\mathbf{R}}$  represents the nuclear degrees of freedom, and  $\langle\cdots\rangle_e$  represents an integral over electronic degrees of freedom [18, 19]. Then, from the coupled time-dependent Schrödinger equations (TDSEs) for  $\chi(\underline{\mathbf{R}}, t)$  and  $|\Phi_{\underline{\mathbf{R}}}(t)\rangle$ , the MQC equations can be derived [21, 29]. The exact classical force for the nuclear trajectory  $\underline{\mathbf{R}}(t)$  is

$$\mathbf{F}_\nu = \dot{\mathbf{P}}_\nu(t) = -\nabla_\nu \tilde{\epsilon} + \dot{\mathbf{A}}_\nu, \quad (1)$$

and the electronic TDSE along the nuclear trajectory is

$$i\hbar \frac{d}{dt} |\Phi_{\underline{\mathbf{R}}}(t)\rangle = \left( \hat{H}_{\text{BO}} + \hat{H}_{\text{ENC}}^{(1)} + \hat{H}_{\text{ENC}}^{(2)} - \tilde{\epsilon} \right) |\Phi_{\underline{\mathbf{R}}}(t)\rangle, \quad (2)$$

where  $\hat{H}_{\text{BO}}$  is the BO Hamiltonian, and  $\mathbf{A}_\nu(\underline{\mathbf{R}}, t) = \langle\Phi_{\underline{\mathbf{R}}}|\hat{p}_\nu|\Phi_{\underline{\mathbf{R}}}\rangle_e$  and  $\tilde{\epsilon}(\underline{\mathbf{R}}, t) = \langle\Phi_{\underline{\mathbf{R}}}(t)|(\hat{H}_{\text{BO}} + \hat{H}_{\text{ENC}}^{(2)} - i\hbar \frac{d}{dt})|\Phi_{\underline{\mathbf{R}}}(t)\rangle_e$  are the time-dependent vector and scalar potentials, respectively. Here,  $\dot{f}$  rep-

resents the total time-derivative  $df/dt$ . The first and second electron-nuclear correlation (ENC) operators are  $\hat{H}_{\text{ENC}}^{(1)} = -\sum_{\nu} \frac{\hbar^2}{2M_{\nu}} \mathcal{P}_{\nu} \cdot \nabla_{\nu} \hat{\Gamma}_{\underline{\mathbf{R}}}$  and  $\hat{H}_{\text{ENC}}^{(2)} = -\sum_{\nu} \frac{\hbar^2}{2M_{\nu}} \left( \nabla_{\nu} \hat{\Gamma}_{\underline{\mathbf{R}}} + \nabla_{\nu} \hat{\Gamma}_{\underline{\mathbf{R}}} \cdot \nabla_{\nu} \hat{\Gamma}_{\underline{\mathbf{R}}} \right)$  where  $\mathcal{P}_{\nu} = \nabla_{\nu} |\chi|^2 / |\chi|^2$  is the total nuclear quantum momentum (QM), and  $\hat{\Gamma}_{\underline{\mathbf{R}}} = |\Phi_{\underline{\mathbf{R}}}\rangle \langle \Phi_{\underline{\mathbf{R}}}|$  is the reduced electron density operator at a nuclear configuration  $\underline{\mathbf{R}}$ . We note that all terms are evaluated along  $\underline{\mathbf{R}}(t)$ .

Further expansion of Eq. (2) in terms of BO basis states  $|\Phi_{\underline{\mathbf{R}}}(t)\rangle = \sum_j C_j |\phi_j\rangle = \sum_j |C_j| e^{iS_j/\hbar} |\phi_j\rangle$  satisfying  $\hat{H}_{\text{BO}} |\phi_j\rangle = \epsilon_j |\phi_j\rangle$  yields

$$\dot{C}_j = \dot{C}_j^{\text{Eh}} + \dot{C}_j^{\text{QM}} + \dot{C}_j^{\text{PQM}} + \dot{C}_j^{\text{Div}} + \dot{C}_j^{\text{Ph}}. \quad (3)$$

For the time evolution of BO coefficients, we have contributions from the Ehrenfest term  $\dot{C}_j^{\text{Eh}} = -\frac{i}{\hbar} \epsilon_j C_j - \sum_{\nu,k} \frac{\mathbf{P}_{\nu}}{M_{\nu}} \cdot \mathbf{d}_{\nu,jk} C_k$ , the QM term  $\dot{C}_j^{\text{QM}} = -\sum_{\nu,k} \frac{\mathbf{P}_{\nu}}{2M_{\nu}} \cdot \mathbf{D}_{\nu,jk} |C_k|^2 C_j$  with  $\mathbf{D}_{\nu,jk} = \nabla_{\nu} S_j - \nabla_{\nu} S_k$ , the PQM [32] term  $\dot{C}_j^{\text{PQM}} = -\sum_{\nu,k} \frac{\mathbf{Q}_{\nu,jk}}{2M_{\nu}} \cdot \mathbf{D}_{\nu,jk} |C_k|^2 C_j$  where  $\mathbf{Q}_{\nu,jk} = \nabla_{\nu} |C_j|^2 / |C_j|^2 + \nabla_{\nu} |C_k|^2 / |C_k|^2$ , the divergence term  $\dot{C}_j^{\text{Div}} = -\sum_{\nu,k} \frac{\nabla_{\nu} \cdot \mathbf{D}_{\nu,jk}}{2M_{\nu}} |C_k|^2 C_j$ , and the phase correction term  $\dot{C}_j^{\text{Ph}} = \frac{i}{\hbar} (\tilde{\epsilon} - \sum_{\nu} \frac{|\nabla_{\nu} S_j - \mathbf{P}_{\nu}|^2}{2M_{\nu}}) C_j$ . Here we neglect the  $O(\hbar^2)$  terms and the nonadiabatic coupling (NAC) terms ( $\mathbf{d}_{\nu,jk} = \langle \phi_j | \nabla_{\nu} \phi_k \rangle_e$  and  $g_{\nu,jk} = \langle \phi_j | \nabla_{\nu}^2 \phi_k \rangle_e$ ) in ENC terms.

The nuclear force [Eq. (1)] in the BO representation can be expressed as

$$\mathbf{F}_{\nu} = \mathbf{F}_{\nu}^{\text{Eh}} + \mathbf{F}_{\nu}^{\text{QM}} + \mathbf{F}_{\nu}^{\text{PQM}} + \mathbf{F}_{\nu}^{\text{Div}} + \mathbf{F}_{\nu}^{\text{Ph}} + \mathbf{F}_{\nu}^{\text{GI}} \quad (4)$$

which directly corresponds to the contributions in Eq. (3) except  $\mathbf{F}_{\nu}^{\text{GI}}$  from the gauge-invariant part of the time-dependent scalar potential,  $\tilde{\epsilon}_{\text{GI}} = \langle \Phi_{\underline{\mathbf{R}}} | \hat{H}_{\text{ENC}}^{(2)} | \Phi_{\underline{\mathbf{R}}} \rangle_e$  in Eq. (1). Detailed derivations for Eqs. (3) and (4) are provided in Supplemental Material [33].

The conventional XF-based MQC approaches, coupled-trajectory MQC (CTMQC) [20–26] or independent-trajectory approaches such as surface hopping dynamics based on XF (SHXF) [27] and Ehrenfest dynamics based on XF (EhXF) [28], only consider  $\dot{C}_j = \dot{C}_j^{\text{Eh}} + \dot{C}_j^{\text{QM}}$  and  $\mathbf{F}_{\nu} = \mathbf{F}_{\nu}^{\text{Eh}} + \mathbf{F}_{\nu}^{\text{QM}}$  obtained from the first ENC operator  $\hat{H}_{\text{ENC}}^{(1)}$  where  $\dot{C}_j^{\text{QM}}$  and  $\mathbf{F}_{\nu}^{\text{QM}}$  provide decoherence with nuclear wave-packet splitting. However, these approaches cannot provide accurate phase evolution [21, 28]. Recently, Arribas and Maitra proposed that an additional correction to the total QM,  $\dot{C}_j^{\text{PQM}}$ , is necessary to consider electronic coherence more accurately [32].

Here we claim that there are more additional terms to be considered at the same or less order as the QM correction, the phase term,  $\dot{C}_j^{\text{Ph}}$ , and the divergence term,  $\dot{C}_j^{\text{Div}}$  which are crucial to describe correct BO phases

and coherence simultaneously. These terms as well as  $\dot{C}_j^{\text{PQM}}$  are derived from the second ENC operator which has been previously overlooked, especially from  $\nabla_{\nu}^2 \hat{\Gamma}_{\underline{\mathbf{R}}}$  in  $\hat{H}_{\text{ENC}}^{(2)}$  [33].

The phase term,  $\dot{C}_j^{\text{Ph}}$ , is of the same order as  $-\frac{i}{\hbar} \epsilon_j C_j$  in  $\dot{C}_j^{\text{Eh}}$ , which governs an additional phase evolution. Here,  $\tilde{\epsilon}$  is a global phase, and can therefore be neglected during time evolution. If we approximate  $\nabla_{\nu} S_i$  by the BO momentum  $\mathbf{P}_{\nu,i} \equiv \alpha_i \mathbf{P}_{\nu}$ , thus  $\mathbf{D}_{\nu,jk} = \mathbf{P}_{\nu,j} - \mathbf{P}_{\nu,k}$ , with  $\alpha_j$  determined by the state-wise total energy conservation condition,  $\alpha_i = \sqrt{\max\left(0, \frac{E_{\text{tot}} - \epsilon_i}{\sum_{\mu} |\mathbf{P}_{\mu,i}|^2 / M_{\mu}}\right)}$ , we obtain

$$\dot{S}_i - \dot{S}_j = -\sum_{\nu} \frac{\mathbf{P}_{\nu,j} - \mathbf{P}_{\nu,k}}{M_{\nu}} \cdot \mathbf{P}_{\nu} \quad (5)$$

from phases in  $\dot{C}_j^{\text{Eh}}$  and  $\dot{C}_j^{\text{Ph}}$ . This shows that the semiclassical phase correction that had previously been introduced in PCSH heuristically [15] is actually an approximation of the phase term of XF. In this context, we expect that the Stückelberg oscillations can be captured with  $\dot{C}_j^{\text{Ph}}$  as PCSH.

The divergence contribution,  $\dot{C}_j^{\text{Div}}$ , contains the divergence  $\mathbf{D}_{\nu,jk}$ , which requires the second derivatives of phases. Despite the difficulty to obtain the second derivatives, the  $\dot{C}_j^{\text{Div}}$  is essential for the conservation of BO population in the absence of NAC, i.e.  $\int d\underline{\mathbf{R}} |\dot{C}_j|^2 |\chi|^2 = \int \nabla_{\nu} \cdot (\sum_k |C_j|^2 |C_k|^2 |\chi|^2 \mathbf{D}_{\nu,jk}) = 0$ , which is obtained from  $\dot{C}_j^{\text{QM}} + \dot{C}_j^{\text{PQM}} + \dot{C}_j^{\text{Div}}$  since  $\dot{C}_j^{\text{Eh}}$  without NAC and  $\dot{C}_j^{\text{Ph}}$  does not contribute to the BO population transfer. Therefore, in this work, we approximate the divergence term using constant pair-wise shift terms (See Supplemental Material [33] for the numerical implementation of the equations).

We benchmark the new equations of motion using the one-dimensional DAG [14] and the 2DNS [15] models. The model Hamiltonians and computational details are provided in the Supplemental Material [33].

Fig. 1 shows the transmission probability on the lower state,  $T_1$ , for the DAG model with various trajectory-based approaches in comparison with the exact wave-packet dynamics. We refer to the results obtained without the additional terms as SHXF and CT, whereas those including the term are denoted as SHXFv2 and CTv2, respectively. The exact behavior shows an increase of oscillation amplitude as  $k_0$  increases, from  $\sim 0.5$  at  $k_0 = 30.0$  a.u. As reported previously, PCSH can correctly reproduce the exact Stückelberg oscillation as aimed [15]. On the other hand, PCSH with the energy-based decoherence correction [11] (PCSH-EDC) removes the oscillation due to over-decoherence. Similarly, CT, which only account for the decoherence, shows  $T_1 \sim 0.5$  for all values of  $k_0$ . Although SHXF shows an oscillatory behavior with respect to  $k_0$ , it deviates from the exact behavior. CTv2 and SHXFv2 recover the correct Stückelberg oscillation.

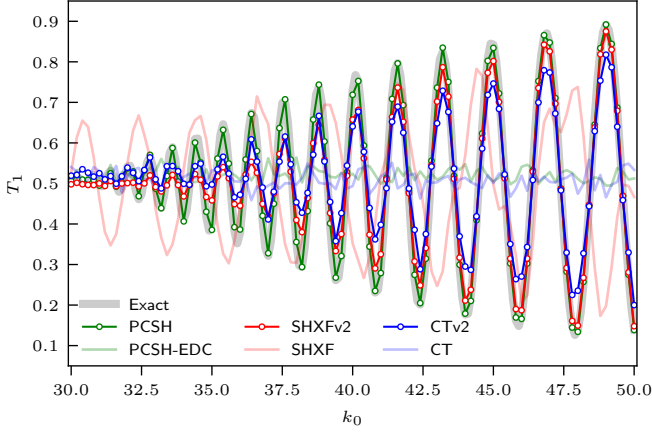


FIG. 1. Transmission probability for the lower state ( $T_1$ ) as a function of initial momentum  $k_0$  for various dynamics methods.  $T_1$  is obtained as  $T_1 = \int_0^\infty dR |\chi_1(R, t_f)|^2$  for the exact wave-packet dynamics and  $T_1 = \sum_{I \in \{R^{(I)}(t_f) > 0\}} |C_1^{(I)}(t_f)|^2 / N_{\text{traj}}$  for the trajectory-based dynamics.  $R^{(I)}(t)$  and  $t_f$  denote the trajectory as a function of time  $t$  and the final time of a simulation, respectively, with the total number of trajectories  $N_{\text{traj}}$ .

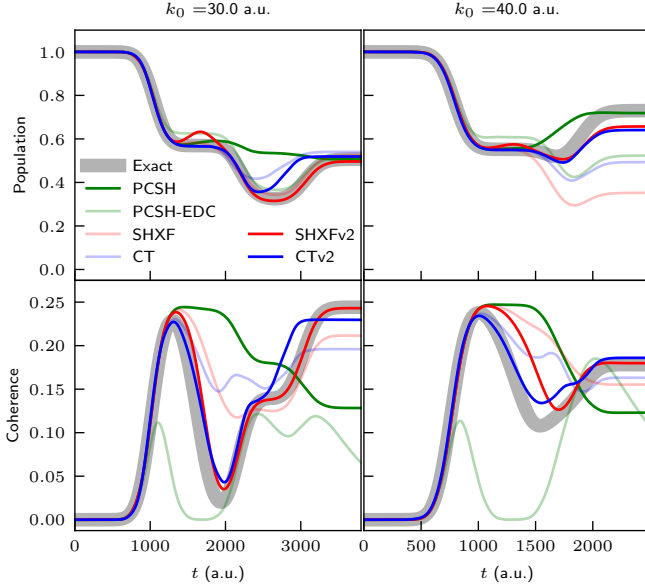


FIG. 2. Time evolution of BO population  $\langle |C_1|^2 \rangle(t)$  (upper) and coherence  $\langle |C_1 C_2|^2 \rangle(t)$  (lower) with different initial momenta  $k_0 = 30$  and  $40$  a.u.

While CTv2 slightly underestimates the overall amplitude, SHXFv2 shows excellent agreement with the exact result at high  $k_0$ , and is qualitatively correct at low  $k_0$ . This demonstrates that the additional phase correction term is essential for the correct time evolution of BO phases.

Although reproducing the correct oscillation in  $T_1$  is encouraging, it remains essential to evaluate the time propagation of wave packets to fully assess the accuracy.

Fig. 2 shows the time evolution of BO population for the lower state,  $\langle |C_1|^2 \rangle(t)$ , and coherence,  $\langle |C_1 C_2|^2 \rangle(t)$ , with different initial momenta  $k_0 = 30.0$  and  $50.0$  a.u. For exact wave-packet dynamics,  $\langle O \rangle(t)$  is defined as  $\langle O \rangle(t) = \int d\mathbf{R} O(\mathbf{R}, t)$ , whereas  $\langle O \rangle(t) \equiv \sum_I^{N_{\text{traj}}} O^{(I)}(t) / N_{\text{traj}}$  is used for MQC methods. Since the DAG model contains two NAC regions, the initial population drop corresponds to passage through the first region, while the separated wave packets on upper and lower states afterward encounter the second region at different times.

PCSH reproduces the final BO populations well but fails to capture the intermediate dynamics for  $k_0 = 30.0$  and shows overcoherence for all  $k_0$  due to the absence of a decoherence correction. In contrast, PCSH-EDC exhibits over-decoherence, yielding final  $\langle |C_1|^2 \rangle$  to  $\sim 0.5$  for all  $k_0$ . All XF-based MQC methods reasonably reproduce the correct BO population dynamics for  $k_0 = 30.0$  a.u. Notably, only CTv2 and SHXFv2 reproduce the accurate intermediate decoherence at  $t \sim 2000$  a.u., highlighting the importance of the additional terms in CTv2 and SHXFv2. For  $k_0 = 40.0$  a.u., CT incorrectly predicts the final population to  $\sim 0.5$ , while SHXF yields the opposite direction of second population transfer. Again, SHXFv2 and CTv2 successfully reproduce the correct BO population and coherence dynamics, including the population transfer at the second NAC region. In these cases, CTv2 provides better coherence between the first and second NAC regions, whereas SHXFv2 exhibits slight overcoherence.

In addition, to analyze the wave-packet dynamics, we construct the spatial distribution of the BO-projected time-dependent nuclear densities,  $|\chi_i(R, t)|^2$ , and BO populations,  $|C_i(R, t)|^2$ , for the DAG model.  $|\chi_i(R, t)|^2$  are obtained from histograms of nuclear trajectories weighted by their corresponding BO populations, while  $|C_i(R, t)|^2$  are calculated by  $|C_i(R, t)|^2 = |\chi_i(R, t)|^2 / |\chi(R, t)|^2$  where the total nuclear density,  $|\chi(R, t)|^2$ , is the histograms of trajectories. Fig. 3 presents  $|\chi_i(R, t)|^2$  and  $|C_i(R, t)|^2$  from the XF-based approaches for large  $k_0$  ( $k_0 = 50$  a.u.), at  $t = 1300$  a.u. (arrival of nuclear wave packets at the second NAC region) and  $t = 1900$  a.u. (after passage through the second NAC region). We observe a marked improvement in the spatial distributions with CTv2 and SHXFv2. CT exhibits oscillatory behavior arising from incorrect phase estimation in each BO state, while SHXF yields an overall inaccurate spatial distribution. By contrast, CTv2 reproduces almost identical results to the exact dynamics. SHXFv2 performs reasonably well at  $k = 1900$  a.u., but at  $k = 1300$  a.u. it produces strongly overlapping nuclear wave packets, likely due to a less accurate treatment of decoherence.

For  $k_0 = 30.0$  a.u., the nuclear wave-packet splitting and the electronic decoherence effects are pronounced after passing the first NAC region because of the small kinetic energy, due to a larger relative difference in the

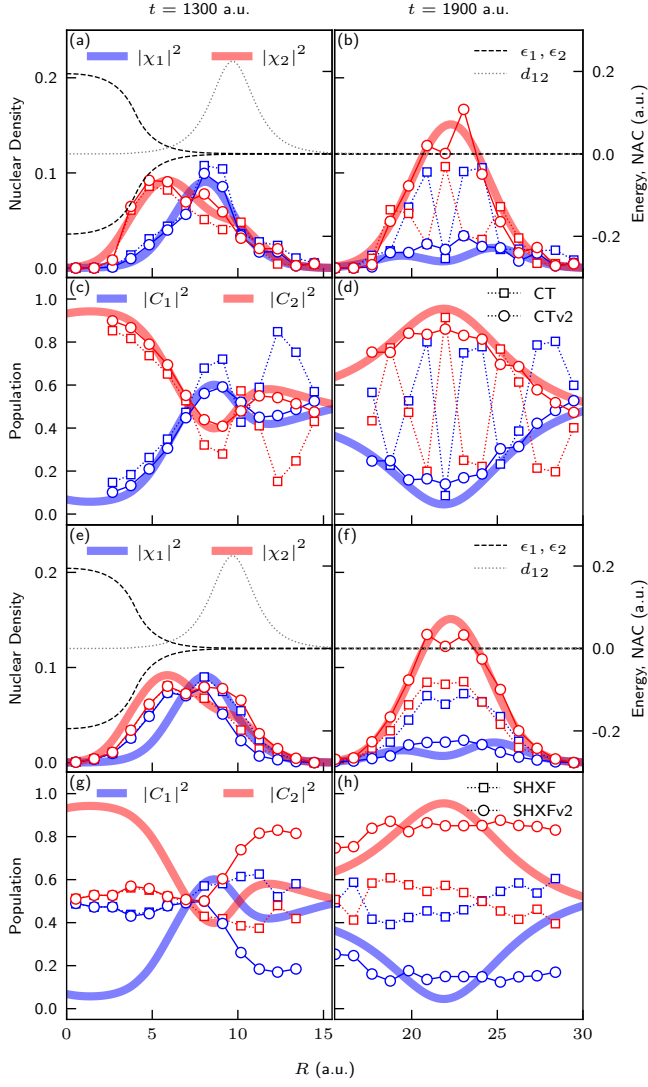


FIG. 3. Spatial distribution of nuclear wave packets ( $|\chi_i(R, t)|^2$ ) and BO populations ( $|C_i(R, t)|^2$ ) at different time steps,  $t = 1300$  a.u. (a,c,e,g) and  $1900$  a.u. (b,d,f,h) with the initial momentum  $k_0 = 50.0$  a.u. for CT-based approaches (CT/CTv2) (a-d) and SHXF-based approaches (SHXF/SHXFv2) (e-h). The BO potential energies  $\epsilon_{1/2}$  and the NAC  $d_{12}$  are depicted to interpret wave-packet dynamics (a,b,e,f).

velocities of nuclear wave packets on different BO states. Thus, the well-separated nuclear wave packets pass the second NAC region sequentially. Fig. 4 shows nuclear wave packets and BO populations at  $t = 2200$  a.u. when  $|\chi_1(R, t)|^2$  meets the second NAC region. CTv2 provides better wave-packet splitting and  $|C_i(R, t)|^2$  compared to CT in Fig. S5 [33], while both deviate from the exact result. On the other hand, the CTv2 with the exact QM and PQM recovers the correct  $|\chi_i(R, t)|^2$  and  $|C_i(R, t)|^2$ , whereas CT [Fig. S5] with the exact QM still deviates from the exact result [33]. Thus, the formula-

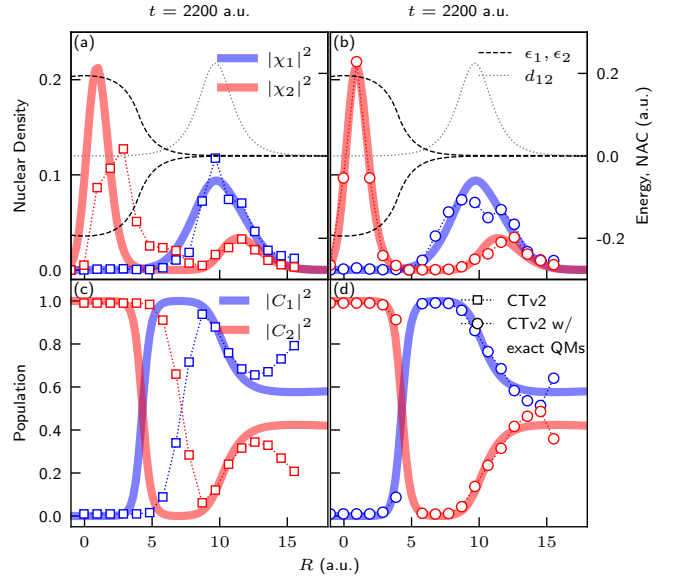


FIG. 4. Spatial distribution of nuclear wave packets (a,b) and BO populations (c,d) at  $t = 2200$  a.u. with the initial momentum  $k_0 = 30.0$  a.u. for CTv2 (a,c) and CTv2 with the QM  $\mathcal{P}_\nu$  and the PQM  $\mathcal{Q}_\nu$  obtained from quantum dynamics (b,d). BO potentials and NAC are depicted as in Fig. 3.

tion is valid; the discrepancies mainly originate from the approximations to  $\mathcal{P}_\nu$  and  $\mathcal{Q}_{\nu,ik}$ , as the true  $|\chi_2(R, t)|^2$  becomes strongly non-Gaussian after the first NAC region for  $k_0 = 30.0$  a.u.

The results from other approaches are provided in Figs. S5–S11 [33]. For all  $k_0$ , PCSH and PCSH-EDC yields either incorrect spatial decoherence or incorrect BO population after the second NAC region, respectively, whereas CTv2 and SHXFv2 exhibit clear enhancement compared to the other methods.

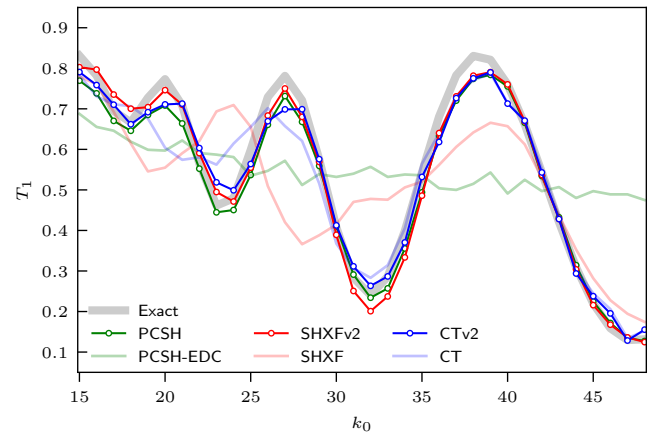


FIG. 5. Transmission probability for the lower state ( $T_1$ ) for the 2DNS model, as in Fig. 1.

Finally, to test the additional corrections in higher-dimensional systems, we compute the  $T_1$  for the 2DNS

model. As shown in Fig. 5, SHXFv2 and CTv2, along with PCSH, reproduce the correct oscillation pattern, whereas PCSH-EDC and SHXF fail, consistent with the DAG results. CT works for  $k_0 > 25$  a.u. but fails for  $k_0 = 17\text{--}25$  a.u. Thus, the phase and PQM corrections enable us to reproduce the quantum dynamics even in higher dimensions.

In this work, we developed new mixed quantum-classical equations of motion for molecules within the exact factorization formalism. The derivation reveals that additional terms of the same or smaller order in  $\hbar$  naturally arise from the full electron-nuclear correlation. In contrast to existing correction schemes, where decoherence and phase adjustments are often introduced heuristically and separately, the exact factorization framework provides both effects simultaneously and without ad hoc assumptions. The newly identified terms consist of the projected quantum momentum, which governs decoherence by correctly separating electronic populations, and a phase-correction term, which ensures accurate phase evolution of the nuclear wave packets.

Numerical benchmarks on representative one- and two-dimensional models demonstrate that these corrections are indispensable for reproducing key features of quantum dynamics, including Stückelberg oscillations, intermediate-time (de)coherence, and the correct spatial distribution of nuclear wave packets. In particular, the enhanced performance of CTv2 and SHXFv2 underscores the importance of explicitly including both decoherence and phase corrections when simulating coupled electron-nuclear motion. Thus, our results establish that the exact factorization formalism provides not only a rigorous foundation for trajectory-based dynamics but also a systematic pathway for deriving corrections that capture the full scope of electron-nuclear correlation effects.

This research was supported by the National Research Foundation of Korea (NRF) funded by the Korean government (Ministry of Science and ICT (MSIT)) (RS-2023-NR119931, RS-2023-00257666, RS-2024-00455131).

---

\* skmin@unist.ac.kr

- [1] A. D. McLachlan, A variational solution of the time-dependent Schrodinger equation, *Mol. Phys.* **8**, 39 (1964).
- [2] J. C. Tully, Molecular dynamics with electronic transitions, *J. Chem. Phys.* **93**, 1061 (1990).
- [3] R. Crespo-Otero and M. Barbatti, Recent advances and perspectives on nonadiabatic mixed quantum-classical dynamics, *Chem. Rev.* **118**, 7026 (2018).
- [4] T. Linker, K. ichi Nomura, A. Aditya, S. Fukushima, R. K. Kalia, A. Krishnamoorthy, A. Nakano, P. Rajak, K. Shimmura, F. Shimojo, and P. Vashishta, Exploring far-from-equilibrium ultrafast polarization control in ferroelectric oxides with excited-state neural network quantum molecular dynamics, *Sci. Adv.* **8**, eabk2625 (2022).
- [5] K. Gope, E. Livshits, D. M. Bittner, R. Baer, and D. Strasser, An “inverse” harpoon mechanism, *Sci. Adv.* **8**, eabq8084 (2022).
- [6] R. Dagar, W. Zhang, P. Rosenberger, T. M. Linker, A. Sousa-Castillo, M. Neuhaus, S. Mitra, S. Biswas, A. Feinberg, A. M. Summers, A. Nakano, P. Vashishta, F. Shimojo, J. Wu, C. C. Vera, S. A. Maier, E. Cortés, B. Bergues, and M. F. Kling, Tracking surface charge dynamics on single nanoparticles, *Sci. Adv.* **10**, eadp1890 (2024).
- [7] K. D. Borne, J. C. Cooper, M. N. R. Ashfold, J. Bachmann, S. Bhattacharyya, R. Boll, M. Bonanomi, M. Bosch, C. Callegari, M. Centurion, M. Coreno, B. F. E. Curchod, M. B. Danailov, A. Demidovich, M. Di Fraia, B. Erk, D. Faccialà, R. Feifel, R. J. G. Forbes, C. S. Hansen, D. M. P. Holland, R. A. Ingle, R. Lindh, L. Ma, H. G. McGhee, S. B. Muvva, J. P. F. Nunes, A. Odate, S. Pathak, O. Plekan, K. C. Prince, P. Rebernik, A. Rouzée, A. Rudenko, A. Simoncig, R. J. Squibb, A. S. Venkatachalam, C. Vozzi, P. M. Weber, A. Kirrander, and D. Rolles, Ultrafast electronic relaxation pathways of the molecular photoswitch quadricyclane, *Nat. Chem.* **16**, 499 (2024).
- [8] Y.-P. Chang, T. Balciunas, Z. Yin, M. Sapunar, B. N. C. Tenorio, A. C. Paul, S. Tsuru, H. Koch, J.-P. Wolf, S. Coriani, and H. J. Wörner, Electronic dynamics created at conical intersections and its dephasing in aqueous solution, *Nat. Phys.* **21**, 137 (2025).
- [9] I. S. Lee, M. Filatov, and S. K. Min, Dynamics of a light-driven molecular rotary motor in an optical cavity, *Nat. Commun.* **16**, 4554 (2025).
- [10] C. Zhu, S. Nangia, A. W. Jasper, and D. G. Truhlar, Coherent switching with decay of mixing: An improved treatment of electronic coherence for non-Born-Oppenheimer trajectories, *J. Chem. Phys.* **121**, 7658 (2004).
- [11] G. Granucci and M. Persico, Critical appraisal of the fewest switches algorithm for surface hopping, *J. Chem. Phys.* **126**, 134114 (2007).
- [12] J. Xu and L. Wang, Branching corrected surface hopping: Resetting wavefunction coefficients based on judgement of wave packet reflection, *J. Chem. Phys.* **150**, 164101 (2019).
- [13] C. Shao, Z. Shi, J. Xu, and L. Wang, Learning decoherence time formulas for surface hopping from quantum dynamics, *J. Phys. Chem. Lett.* **14**, 7680 (2023).
- [14] J. E. Subotnik and N. Shenvi, A new approach to decoherence and momentum rescaling in the surface hopping algorithm, *J. Chem. Phys.* **134**, 024105 (2011).
- [15] N. Shenvi, J. E. Subotnik, and W. Yang, Phase-corrected surface hopping: Correcting the phase evolution of the electronic wavefunction, *J. Chem. Phys.* **135**, 024101 (2011).
- [16] J. R. Mannouch and J. O. Richardson, A mapping approach to surface hopping, *J. Chem. Phys.* **158**, 104111 (2023).
- [17] B. Wu, B. Li, X. He, X. Cheng, J. Ren, and J. Liu, Nonadiabatic field: A conceptually novel approach for nonadiabatic quantum molecular dynamics, *J. Chem. Theory Comput.* **21**, 3775 (2025).
- [18] A. Abedi, N. T. Maitra, and E. K. U. Gross, Exact Factorization of the Time-Dependent Electron-Nuclear Wave Function, *Phys. Rev. Lett.* **105**, 123002 (2010).
- [19] A. Abedi, N. T. Maitra, and E. K. U. Gross, Correlated electron-nuclear dynamics: Exact factorization of

- the molecular wavefunction, *J. Chem. Phys.* **137**, 22A530 (2012).
- [20] S. K. Min, F. Agostini, and E. K. U. Gross, Coupled-Trajectory Quantum-Classical Approach to Electronic Decoherence in Nonadiabatic Processes, *Phys. Rev. Lett.* **115**, 073001 (2015).
  - [21] F. Agostini, S. K. Min, A. Abedi, and E. K. U. Gross, Quantum-Classical Nonadiabatic Dynamics: Coupled-vs Independent-Trajectory Methods, *J. Chem. Theory Comput.* **12**, 2127 (2016).
  - [22] G. H. Gossel, F. Agostini, and N. T. Maitra, Coupled-Trajectory Mixed Quantum-Classical Algorithm: A Deconstruction, *J. Chem. Theory Comput.* **14**, 4513 (2018).
  - [23] F. Talotta, S. Morisset, N. Rougeau, D. Lauvergnat, and F. Agostini, Internal Conversion and Intersystem Crossing with the Exact Factorization, *J. Chem. Theory Comput.* **16**, 4833 (2020).
  - [24] C. Pieroni and F. Agostini, Nonadiabatic Dynamics with Coupled Trajectories, *J. Chem. Theory Comput.* **17**, 5969 (2021).
  - [25] E. V. Arribas and N. T. Maitra, Energy-conserving coupled trajectory mixed quantum-classical dynamics, *J. Chem. Phys.* **158**, 161105 (2023).
  - [26] E. Sangiorgio Gil, D. Lauvergnat, and F. Agostini, Exact factorization of the photon-electron-nuclear wavefunction: Formulation and coupled-trajectory dynamics, *J. Chem. Phys.* **161**, 084112 (2024).
  - [27] J.-K. Ha, I. S. Lee, and S. K. Min, Surface Hopping Dynamics beyond Nonadiabatic Couplings for Quantum Coherence, *J. Phys. Chem. Lett.* **9**, 1097 (2018).
  - [28] J.-K. Ha and S. K. Min, Independent trajectory mixed quantum-classical approaches based on the exact factorization, *J. Chem. Phys.* **156**, 174109 (2022).
  - [29] D. Han, J.-K. Ha, and S. K. Min, Real-Space and Real-Time Propagation for Correlated Electron-Nuclear Dynamics Based on Exact Factorization, *J. Chem. Theory Comput.* **19**, 2186 (2023).
  - [30] L. Dupuy, A. Rikus, and N. T. Maitra, Exact-Factorization-Based Surface Hopping without Velocity Adjustment, *J. Phys. Chem. Lett.* **15**, 2643 (2024).
  - [31] D. Han, C. C. Martens, and A. V. Akimov, Generalization of Quantum-Trajectory Surface Hopping to Multiple Quantum States, *J. Chem. Theory Comput.* **21**, 2839 (2025).
  - [32] E. V. Arribas and N. T. Maitra, Electronic Coherences in Molecules: The Projected Nuclear Quantum Momentum as a Hidden Agent, *Phys. Rev. Lett.* **133**, 233201 (2024).
  - [33] See Supplemental Material at [URL will be inserted by publisher] for the derivation of the equations and their numerical implementation, the computational details of numerical tests, and additional numerical test results.
  - [34] M. Feit, J. Fleck, and A. Steiger, Solution of the Schrödinger equation by a spectral method, *J. Comput. Phys.* **47**, 412 (1982).

# Supplemental Material for "Unifying Decoherence and Phase Evolution in Mixed Quantum–Classical Dynamics through Exact Factorization"

Jong-Kwon Ha,<sup>1</sup> Seong Ho Kim,<sup>2</sup> and Seung Kyu Min<sup>2,\*</sup>

<sup>1</sup>*Department of Chemistry, Dalhousie University,  
6274 Coburg Rd, Halifax, NS B3H 4R2, Canada*

<sup>2</sup>*Department of Chemistry, Ulsan National Institute of Science and Technology (UNIST),  
50 UNIST-gil, Ulsu-gun, Ulsan 44919, South Korea*

(Dated: November 11, 2025)

## I. EXACT MIXED QUANTUM-CLASSICAL EQUATIONS OF MOTION IN THE BORN-OPPENHEIMER REPRESENTATION

### A. Electronic time-dependent Schrödinger equation

If we expand the electronic state with the Born-Oppenheimer (BO) basis states in the electronic time-dependent Schrödinger equation (TDSE) for the exact mixed quantum-classical (MQC) dynamics, we get

$$\frac{d}{dt}C_j^{(I)} = -\frac{i}{\hbar}\epsilon_j^{(I)}C_j^{(I)} - \sum_k \sum_\nu \frac{\mathbf{P}_\nu^{(I)}}{M_\nu} \cdot \mathbf{d}_{\nu,ik}^{(I)}C_k^{(I)} - \frac{i}{\hbar}\tilde{\epsilon}^{(I)}C_j^{(I)} \quad (\text{S1a})$$

$$+ \sum_\nu \frac{i\hbar}{2M_\nu} \mathcal{P}_\nu^{(I)} \cdot \left( \nabla_\nu C_j + \sum_k C_k \mathbf{d}_{\nu,jk} - \frac{i}{\hbar} \mathbf{A}_\nu C_j \right)^{(I)} \quad (\text{S1b})$$

$$+ \sum_\nu \frac{i\hbar}{2M_\nu} \left( \nabla_\nu^2 C_j + 2 \sum_k \nabla_\nu C_k \mathbf{d}_{\nu,jk} + \sum_k C_k g_{\nu,jk} - 2 \frac{i}{\hbar} \mathbf{A}_\nu \cdot \nabla_\nu C_j - 2 \frac{i}{\hbar} \mathbf{A}_\nu \cdot \sum_k C_k \mathbf{d}_{\nu,jk} \right)^{(I)} \quad (\text{S1c})$$

$$+ \sum_\nu \frac{i\hbar}{2M_\nu} \left( \sum_k \nabla_\nu C_k^* C_k + 2 \sum_{kl} \nabla_\nu C_k^* C_l \mathbf{d}_{\nu,lk}^* + \nabla_\nu C_k^* C_l g_{\nu,lk}^* \right)^{(I)} C_j^{(I)} \quad (\text{S1d})$$

$$+ \sum_\nu \frac{i\hbar}{2M_\nu} \left( \sum_k |\nabla_\nu C_k|^2 + \sum_{kl} \nabla_\nu C_k^* C_l \mathbf{d}_{\nu,kl} + \sum_{kl} C_k^* \nabla_\nu C_l \mathbf{d}_{\nu,lk}^* + \sum_{kl} C_k^* C_l \langle \nabla_\nu \phi_k | \nabla_\nu \phi_l \rangle - \frac{1}{\hbar^2} |\mathbf{A}_\nu|^2 \right)^{(I)} C_j^{(I)}, \quad (\text{S1e})$$

where  $\mathbf{d}_{\nu,kl} = \langle \phi_k | \nabla_\nu \phi_l \rangle_{\underline{\mathbf{r}}}$  and  $g_{\nu,kl} = \langle \phi_k | \nabla_\nu^2 \phi_l \rangle_{\underline{\mathbf{r}}}$  are first and second order nonadiabatic couplings (NACs). The line (S1a) contains the Ehrenfest term plus time-dependent scalar potential contribution, (S1b) is from  $\hat{H}_{\text{ENC}}^{(1)}$ , (S1c) and (S1d) are from  $\nabla_\nu^2 \hat{\Gamma}_{\underline{\mathbf{R}}}$  term of  $\hat{H}_{\text{ENC}}^{(2)}$ , and (S1e) is from  $\nabla_\nu \hat{\Gamma}_{\underline{\mathbf{R}}} \cdot \nabla_\nu \hat{\Gamma}_{\underline{\mathbf{R}}}$  term of  $\hat{H}_{\text{ENC}}^{(2)}$ . Neglecting NACs and writing

---

\* skmin@unist.ac.kr

the BO coefficients in polar form, we can write the equation as

$$\begin{aligned}
\frac{d}{dt}C_j^{(I)} = & -\frac{i}{\hbar}\epsilon_j^{(I)}C_j^{(I)} - \sum_k \sum_\nu \frac{\mathbf{P}_\nu^{(I)}}{M_\nu} \cdot \mathbf{d}_{\nu,ik}^{(I)} C_k^{(I)} - \frac{i}{\hbar}\tilde{\epsilon}^{(I)}C_j^{(I)} \\
& - \sum_\nu \frac{1}{2M_\nu} \mathcal{P}_\nu^{(I)} \cdot (\nabla_\nu S_j - \mathbf{A}_\nu)^{(I)} C_j^{(I)} + \sum_\nu \frac{i\hbar}{2M_\nu} \mathcal{P}_\nu^{(I)} \cdot \frac{\nabla_\nu |C_j|}{|C_j|} C_j \\
& - \sum_\nu \frac{1}{2M_\nu} \sum_k \left( 2 \frac{\nabla_\nu |C_j|}{|C_j|} \cdot \nabla_\nu S_j + \nabla_\nu^2 S_j - 2 \frac{\nabla_\nu |C_j|}{|C_j|} \cdot \mathbf{A}_\nu - \frac{\nabla_\nu |C_k|}{|C_k|} \cdot \nabla_\nu S_k - \nabla_\nu^2 S_k \right)^{(I)} |C_k^{(I)}|^2 C_j^{(I)} \\
& + \sum_\nu \frac{i\hbar}{2M_\nu} \sum_k \left( \frac{\nabla_\nu^2 |C_j|}{|C_j|} - \frac{1}{\hbar^2} |\nabla_\nu S_j|^2 + \frac{2}{\hbar^2} \nabla_\nu S_j \cdot \mathbf{A}_\nu + \sum_k \frac{\nabla_\nu^2 |C_k|}{|C_k|} - \frac{1}{\hbar^2} |\nabla_\nu S_k|^2 \right)^{(I)} |C_k^{(I)}|^2 C_j^{(I)} \\
& + \sum_\nu \frac{i\hbar}{2M_\nu} \sum_k \left( \frac{\nabla_\nu |C_k|}{|C_k|} \cdot \frac{\nabla_\nu |C_k|}{|C_k|} + \frac{1}{\hbar^2} |\nabla_\nu S_k|^2 - \frac{1}{\hbar^2} |\mathbf{A}_\nu|^2 \right)^{(I)} |C_k^{(I)}|^2 C_j^{(I)}.
\end{aligned} \tag{S2}$$

Using  $\sum_k |C_k| = 1$ ,  $\mathbf{A}_\nu = \sum_k |C_k|^2 \nabla_\nu S_k + \hbar \Im\{C_k^* C_l \mathbf{d}_{\nu,kl}\}$ , and neglecting NAC for  $\mathbf{A}_\nu$ , we get

$$\begin{aligned}
\frac{d}{dt}C_j^{(I)} = & -\frac{i}{\hbar}\epsilon_j^{(I)}C_j^{(I)} - \sum_k \sum_\nu \frac{\mathbf{P}_\nu^{(I)}}{M_\nu} \cdot \mathbf{d}_{\nu,ik}^{(I)} C_k^{(I)} - \frac{i}{\hbar}\tilde{\epsilon}^{(I)}C_j^{(I)} \\
& - \sum_\nu \frac{1}{2M_\nu} \sum_k \left( \mathcal{P}_\nu^{(I)} + \mathcal{Q}_{\nu,jk}^{(I)} + \nabla_\nu \right) \cdot \mathbf{D}_{\nu,jk}^{(I)} |C_k^{(I)}|^2 C_j^{(I)} \\
& + \sum_\nu \frac{i\hbar}{2M_\nu} \sum_k \left( \frac{\nabla_\nu^2 |C_j|}{|C_j|} + \mathcal{P}_\nu^{(I)} \cdot \frac{\nabla_\nu |C_j|}{|C_j|} - \frac{1}{\hbar^2} |\nabla_\nu S_j - \mathbf{A}_\nu|^2 \right)^{(I)} C_j^{(I)},
\end{aligned} \tag{S3}$$

where  $\mathbf{D}_{\nu,jk} = \nabla_\nu S_j - \nabla_\nu S_k$ ,  $\mathcal{P}_\nu = \nabla_\nu |\chi|^2 / |\chi|^2$  is the total nuclear quantum momentum (QM), and  $\mathcal{Q}_{\nu,jk} = \nabla_\nu |C_j|^2 / |C_j|^2 + \nabla_\nu |C_k|^2 / |C_k|^2$  is the reduced projected quantum momentum (PQM) [1]. As a result, the electron-nuclear correlation (ENC) Hamiltonian matrix is diagonal in the absence of NAC, and its real and imaginary part corresponds to decoherence and phase correction, respectively. We note that the new decoherence correction term originates solely from  $\nabla_\nu^2 \hat{\Gamma}_{\underline{\mathbf{R}}}$  where  $\hat{\Gamma}_{\underline{\mathbf{R}}} = |\Phi_{\underline{\mathbf{R}}}\rangle \langle \Phi_{\underline{\mathbf{R}}}|$  is the reduced electron density operator, while  $\nabla_\nu \hat{\Gamma}_{\underline{\mathbf{R}}} \cdot \nabla_\nu \hat{\Gamma}_{\underline{\mathbf{R}}}$  contributes merely to the global phase with cancellations with the phase correction term from  $\nabla_\nu^2 \hat{\Gamma}_{\underline{\mathbf{R}}}$  that just make the equation simpler.

Finally, keeping the lowest order of  $\hbar$  terms, we get the final equation:

$$\begin{aligned}
\frac{d}{dt}C_j^{(I)} = & -\frac{i}{\hbar}\epsilon_j^{(I)}C_j^{(I)} - \sum_k \sum_\nu \frac{\mathbf{P}_\nu^{(I)}}{M_\nu} \cdot \mathbf{d}_{\nu,ik}^{(I)} C_k^{(I)} \\
& - \sum_\nu \frac{1}{2M_\nu} \sum_k \left( \mathcal{P}_\nu^{(I)} + \mathcal{Q}_{\nu,jk}^{(I)} + \nabla_\nu \right) \cdot \mathbf{D}_{\nu,jk}^{(I)} |C_k^{(I)}|^2 C_j^{(I)} \\
& - \frac{i}{\hbar} \left( \sum_\nu \frac{|\nabla_\nu S_j^{(I)} - \mathbf{A}_\nu^{(I)}|^2}{2M_\nu} + \tilde{\epsilon}^{(I)} \right) C_j^{(I)} \\
\equiv & -\frac{i}{\hbar}\epsilon_j^{(I)}C_j^{(I)} - \sum_k \sum_\nu \frac{\mathbf{P}_\nu^{(I)}}{M_\nu} \cdot \mathbf{d}_{\nu,ik}^{(I)} C_k^{(I)} \\
& + \left( \frac{1}{\hbar} H_j^{\text{DC}} - \frac{i}{\hbar} H_j^{\text{PC}} \right) C_j^{(I)}
\end{aligned} \tag{S4}$$

for the electronic TDSE in the BO representation.



## B. Nuclear force

The nuclear force is

$$\begin{aligned}
\mathbf{F}_\nu^{(I)}(t) &= -\nabla_\nu \tilde{\epsilon}^{(I)} + \dot{\mathbf{A}}_\nu^{(I)} \\
&= -\nabla_\nu \left( \langle \Phi_{\underline{\mathbf{R}}} | \hat{H}_{\text{BO}} | \Phi_{\underline{\mathbf{R}}} \rangle_{\underline{\mathbf{r}}} + \sum_\mu \frac{\hbar^2 \langle \nabla_\mu \Phi_{\underline{\mathbf{R}}} | \nabla_\mu \Phi_{\underline{\mathbf{R}}} \rangle_{\underline{\mathbf{r}}} - |\mathbf{A}_\mu|^2}{2M_\mu} \right)^{(I)} + 2\Re \left( i\hbar \langle \nabla_\nu \Phi_{\underline{\mathbf{R}}} | \frac{d}{dt} \Phi_{\underline{\mathbf{R}}} \rangle_{\underline{\mathbf{r}}} \right)^{(I)} \\
&= -\nabla_\nu \left( \langle \Phi_{\underline{\mathbf{R}}} | \hat{H}_{\text{BO}} | \Phi_{\underline{\mathbf{R}}} \rangle_{\underline{\mathbf{r}}} + \sum_\mu \frac{\hbar^2 \langle \nabla_\mu \Phi_{\underline{\mathbf{R}}} | \nabla_\mu \Phi_{\underline{\mathbf{R}}} \rangle_{\underline{\mathbf{r}}} - |\mathbf{A}_\mu|^2}{2M_\mu} \right)^{(I)} + 2\Re \left( \langle \nabla_\nu \Phi_{\underline{\mathbf{R}}} | (\hat{H}_{\text{BO}} + \hat{H}_{\text{ENC}} - \tilde{\epsilon}) | \Phi_{\underline{\mathbf{R}}} \rangle_{\underline{\mathbf{r}}} \right) \\
&= -\langle \Phi_{\underline{\mathbf{R}}} | \nabla_\nu \hat{H}_{\text{BO}} | \Phi_{\underline{\mathbf{R}}} \rangle_{\underline{\mathbf{r}}}^{(I)} - \nabla_\nu \left( \sum_\mu \frac{\hbar^2 \langle \nabla_\mu \Phi_{\underline{\mathbf{R}}} | \nabla_\mu \Phi_{\underline{\mathbf{R}}} \rangle_{\underline{\mathbf{r}}} - |\mathbf{A}_\mu|^2}{2M_\mu} \right)^{(I)} + 2\Re \left( \langle \nabla_\nu \Phi_{\underline{\mathbf{R}}} | \hat{H}_{\text{ENC}} | \Phi_{\underline{\mathbf{R}}} \rangle_{\underline{\mathbf{r}}} \right)^{(I)}.
\end{aligned} \tag{S5}$$

The full nuclear force, including all NAC contributions within the ENC formalism, can be derived by straightforward but lengthy algebra involving numerous terms. For brevity, and because the NACs are generally highly localized in the nuclear configuration space, these contributions are neglected in the following. As a result, the  $H_{\text{ENC}}$  is diagonal in the BO expansion in the absence of NACs, the last term in the above equation becomes

$$\begin{aligned}
2\Re \left( \sum_k \nabla_\nu C_k^* H_k^{\text{ENC}} C_k \right)^{(I)} &= 2\Re \left\{ \sum_k \nabla_\nu C_k^* (iH_k^{\text{DC}} + H_k^{\text{PC}}) C_k \right\}^{(I)} \\
&= 2\Re \left\{ \sum_k \left( \frac{\nabla_\nu |C_k|}{|C_k|} - \frac{i}{\hbar} \nabla_\nu S_k \right) (iH_k^{\text{DC}} + H_k^{\text{PC}}) |C_k|^2 \right\}^{(I)} \\
&= 2 \left\{ \sum_k \left( \frac{1}{\hbar} \nabla_\nu S_k H_k^{\text{DC}} + \frac{\nabla_\nu |C_k|}{|C_k|} H_k^{\text{PC}} \right) |C_k|^2 \right\}^{(I)}.
\end{aligned} \tag{S6}$$

Then, the nuclear force in the BO representation becomes

$$\begin{aligned}
\mathbf{F}_\nu &= -\sum_k |C_k|^2 \nabla_\nu \epsilon_k - \sum_{k,l} C_k C_l^* (\epsilon_k - \epsilon_l) \mathbf{d}_{\nu,kl} - \nabla_\nu \left( \sum_\mu \frac{\hbar^2 \langle \nabla_\mu \Phi_{\underline{\mathbf{R}}} | \nabla_\mu \Phi_{\underline{\mathbf{R}}} \rangle_{\underline{\mathbf{r}}} - |\mathbf{A}_\mu|^2}{2M_\mu} \right) \\
&\quad - \sum_{k,l} \mathbf{D}_{\nu,kl} \left\{ \sum_\mu \frac{1}{2M_\mu} (\mathcal{P}_\mu + \mathcal{Q}_{\mu,kl} + \nabla_\mu) \cdot \mathbf{D}_{\mu,kl} \right\} |C_l|^2 |C_k|^2 \\
&\quad + 2 \sum_k \frac{\nabla_\nu |C_k|}{|C_k|} \left( -\tilde{\epsilon} + \sum_\mu \frac{|\nabla_\mu S_k - \mathbf{A}_\mu|^2}{2M_\mu} \right) |C_k|^2.
\end{aligned} \tag{S7}$$

We omit  $(I)$  for brevity in this subsection. Since  $\sum_k |C_k| \nabla_\nu |C_k| = \nabla_\nu (\sum_k |C_k|^2)/2 = 0$ ,  $\sum_k |C_k| \nabla_\nu |C_k| \tilde{\epsilon} = 0$  meaning that there is no contribution from the global phase on the nuclear force,

$$\begin{aligned}
\mathbf{F}_\nu &= -\sum_k |C_k|^2 \nabla_\nu \epsilon_k - \sum_{k,l} C_k C_l^* (\epsilon_k - \epsilon_l) \mathbf{d}_{\nu,kl} - \nabla_\nu \left( \sum_\mu \frac{\hbar^2 \langle \nabla_\mu \Phi_{\underline{\mathbf{R}}} | \nabla_\mu \Phi_{\underline{\mathbf{R}}} \rangle_{\underline{\mathbf{r}}} - |\mathbf{A}_\mu|^2}{2M_\mu} \right) \\
&\quad - \sum_{k,l} \mathbf{D}_{\nu,kl} \left\{ \sum_\mu \frac{1}{2M_\mu} (\mathcal{P}_\mu + \mathcal{Q}_{\mu,kl} + \nabla_\mu) \cdot \mathbf{D}_{\mu,kl} \right\} |C_l|^2 |C_k|^2 \\
&\quad + \sum_k \frac{\nabla_\nu |C_k|}{|C_k|} \left( \sum_\mu \frac{|\nabla_\mu S_k - \mathbf{A}_\mu|^2}{M_\mu} \right) |C_k|^2
\end{aligned} \tag{S8}$$

The last term from PC can be rearranged

$$\begin{aligned}
\sum_k \frac{\nabla_\nu |C_k|}{|C_k|} \left( \sum_\mu \frac{|\nabla_\mu S_k - \mathbf{A}_\mu|^2}{M_\mu} \right) |C_k|^2 &= \sum_k \frac{\nabla_\nu |C_k|}{|C_k|} \left( \sum_\mu \frac{|\nabla_\mu S_k|^2 + |\mathbf{A}_\mu|^2 - 2\nabla_\mu S_k \cdot \mathbf{A}_\mu}{M_\mu} \right) |C_k|^2 \\
&= \sum_k \frac{\nabla_\nu |C_k|}{|C_k|} \left( \sum_\mu \frac{|\nabla_\mu S_k|^2 - 2\nabla_\mu S_k \cdot \mathbf{A}_\mu}{M_\mu} \right) |C_k|^2 \\
&= \sum_k \frac{\nabla_\nu |C_k|}{|C_k|} \left( \sum_\mu \frac{|\nabla_\mu S_k|^2 + \sum_l |C_l|^2 |\nabla_\mu S_l|^2 - 2\nabla_\mu S_k \cdot \sum_l |C_l|^2 \nabla_\mu S_l}{M_\mu} \right) |C_k|^2 \\
&= \sum_{k,l} \frac{\nabla_\nu |C_k|}{|C_k|} \left( \sum_\mu \frac{|\nabla_\mu S_k - \nabla_\mu S_l|^2}{M_\mu} \right) |C_k|^2 |C_l|^2,
\end{aligned} \tag{S9}$$

where we use  $\sum_k |C_k|^2 = 1$  and  $\sum_k |C_k| \nabla_\nu |C_k| = \nabla_\nu (\sum_k |C_k|^2)/2 = 0$ , and neglected NAC in  $\mathbf{A}_\mu$  again. As a result,

$$\begin{aligned}
\mathbf{F}_\nu &= - \sum_k |C_k|^2 \nabla_\nu \epsilon_k - \sum_{k,l} C_k C_l^* (\epsilon_k - \epsilon_l) \mathbf{d}_{\nu,kl} - \nabla_\nu \left( \sum_\mu \frac{\hbar^2 \langle \nabla_\mu \Phi_{\mathbf{R}} | \nabla_\mu \Phi_{\mathbf{R}} \rangle_{\mathbf{r}} - |\mathbf{A}_\mu|^2}{2M_\mu} \right) \\
&\quad - \sum_{k,l} \mathbf{D}_{\nu,kl} \left\{ \sum_\mu \frac{1}{2M_\mu} (\mathcal{P}_\mu + \mathcal{Q}_{\mu,kl} + \nabla_\mu) \cdot \mathbf{D}_{\mu,kl} \right\} |C_l|^2 |C_k|^2 \\
&\quad + \sum_{k,l} \frac{\nabla_\nu |C_k|}{|C_k|} \left( \sum_\mu \frac{|\mathbf{D}_{\mu,kl}|^2}{M_\mu} \right) |C_k|^2 |C_l|^2,
\end{aligned} \tag{S10}$$

where the Ehrenfest force is given by  $\mathbf{F}_\nu^{\text{Eh}} = - \sum_k |C_k|^2 \nabla_\nu \epsilon_k - \sum_{k,l} C_k C_l^* (\epsilon_k - \epsilon_l) \mathbf{d}_{\nu,kl}$ , the force from the QM and the PQM is combined as  $\mathbf{F}_\nu^{\text{QM}} + \mathbf{F}_\nu^{\text{PQM}} = - \sum_{k,l} \mathbf{D}_{\nu,kl} \left( \sum_\mu \frac{\mathcal{P}_\mu + \mathcal{Q}_{\mu,kl}}{2M_\mu} \cdot \mathbf{D}_{\mu,kl} \right) |C_l|^2 |C_k|^2$ , the force from the divergence of  $\mathbf{D}_{\nu,jk}$  is  $\mathbf{F}_\nu^{\text{Div}} = - \sum_{k,l} \mathbf{D}_{\nu,kl} \left( \sum_\mu \frac{\nabla_\mu \cdot \mathbf{D}_{\mu,kl}}{2M_\mu} \right) |C_l|^2 |C_k|^2$ , and the force from the phase correction is  $\mathbf{F}_\nu^{\text{Ph}} = \sum_{k,l} \frac{\nabla_\nu |C_k|}{|C_k|} \left( \sum_\mu \frac{|\mathbf{D}_{\mu,kl}|^2}{M_\mu} \right) |C_k|^2 |C_l|^2$  and  $\mathbf{F}^{\text{GI}} = - \nabla_\nu \left( \sum_\mu \frac{\hbar^2 \langle \nabla_\mu \Phi_{\mathbf{R}} | \nabla_\mu \Phi_{\mathbf{R}} \rangle_{\mathbf{r}} - |\mathbf{A}_\mu|^2}{2M_\mu} \right)$  in Eq (4).

### 1. Nuclear gradient of gauge independent part of time-dependent scalar potential

To expand  $\mathbf{F}_\nu^{\text{GI}}$  with the BO basis, we expand it up to the cartesian coordinates:

$$\begin{aligned}
F_{\nu,q}^{\text{GI}} &= - \partial_{\nu,q} \sum_{\mu,p} \frac{\hbar^2 \langle \partial_{\mu,p} \Phi_{\mathbf{R}} | \partial_{\mu,p} \Phi_{\mathbf{R}} \rangle_{\mathbf{r}} - \hbar^2 \left| \langle \Phi_{\mathbf{R}} | \partial_{\mu,p} \Phi_{\mathbf{R}} \rangle \right|^2}{2M_\mu} \\
&= - \partial_{\nu,q} \sum_{\mu,p} \frac{\hbar^2 \sum_k \partial_{\mu,p} C_k^* \partial_{\mu,p} C_k - \hbar^2 \left| \sum_k C_k^* \partial_{\mu,p} C_k \right|^2}{2M_\mu} \\
&= - \sum_{\mu,p} \frac{\hbar^2}{2M_\mu} \left[ \sum_k 2\Re \{ \partial_{\nu,q} \partial_{\mu,p} C_k^* \partial_{\mu,p} C_k \} - \sum_{k,l} 2\Re \{ (\partial_{\nu,q} C_k^* \partial_{\mu,p} C_k + C_k^* \partial_{\nu,q} \partial_{\mu,p} C_k) (C_l \partial_{\mu,p} C_l^*) \} \right].
\end{aligned} \tag{S11}$$

where  $\{p, q\} \in \{x, y, z\}$ ,  $\partial_{\nu,p} = \partial/\partial p_\nu$ , and again the NAC terms are neglected. The first and second order nuclear gradient of a BO coefficient are

$$\partial_{\nu,q} C_k = \left( \frac{\partial_{\nu,q} |C_k|}{|C_k|} + \frac{i}{\hbar} \partial_{\nu,q} S_k \right) C_k, \tag{S12}$$

and

$$\begin{aligned}\partial_{\nu,q}\partial_{\mu,p}C_k &= \partial_{\nu,q} \left\{ \left( \frac{\partial_{\mu,p}|C_k|}{|C_k|} + \frac{i}{\hbar}\partial_{\mu,p}S_k \right) C_k \right\} \\ &= \left[ \partial_{\nu,q} \left( \frac{\partial_{\mu,p}|C_k|}{|C_k|} + \frac{i}{\hbar}\partial_{\mu,p}S_k \right) \right] C_k + \left( \frac{\partial_{\mu,p}|C_k|}{|C_k|} + \frac{i}{\hbar}\partial_{\mu,p}S_k \right) \left( \frac{\partial_{\nu,q}|C_k|}{|C_k|} + \frac{i}{\hbar}\partial_{\nu,q}S_k \right) C_k,\end{aligned}\tag{S13}$$

respectively, without NACs. Then,

$$\begin{aligned}F_{\nu,q}^{\text{GI}} &= -\sum_{\mu,p} \frac{\hbar^2}{2M_\mu} \left[ \sum_k 2\Re \left\{ \left[ \partial_{\nu,q} \left( \frac{\partial_{\mu,p}|C_k|}{|C_k|} - \frac{i}{\hbar}\partial_{\mu,p}S_k \right) \right] \left( \frac{\partial_{\mu,p}|C_k|}{|C_k|} + \frac{i}{\hbar}\partial_{\mu,p}S_k \right) |C_k|^2 \right. \right. \\ &\quad \left. \left. + \left( \frac{\partial_{\nu,q}|C_k|}{|C_k|} - \frac{i}{\hbar}\partial_{\nu,q}S_k \right) \left( \frac{\partial_{\mu,p}|C_k|}{|C_k|} - \frac{i}{\hbar}\partial_{\mu,p}S_k \right) \left( \frac{\partial_{\mu,p}|C_k|}{|C_k|} + \frac{i}{\hbar}\partial_{\mu,p}S_k \right) |C_k|^2 \right\} \right. \\ &\quad \left. - \sum_{k,l} 2\Re \left\{ \left( \frac{\partial_{\nu,q}|C_k|}{|C_k|} - \frac{i}{\hbar}\partial_{\nu,q}S_k \right) \left( \frac{\partial_{\mu,p}|C_k|}{|C_k|} + \frac{i}{\hbar}\partial_{\mu,p}S_k \right) \left( \frac{\partial_{\mu,p}|C_l|}{|C_l|} - \frac{i}{\hbar}\partial_{\mu,p}S_l \right) |C_k|^2 |C_l|^2 \right. \right. \\ &\quad \left. \left. + \left[ \partial_{\nu,q} \left( \frac{\partial_{\mu,p}|C_k|}{|C_k|} + \frac{i}{\hbar}\partial_{\mu,p}S_k \right) \right] \left( \frac{\partial_{\mu,p}|C_l|}{|C_l|} - \frac{i}{\hbar}\partial_{\mu,p}S_l \right) |C_k|^2 |C_l|^2 \right. \right. \\ &\quad \left. \left. + \left( \frac{\partial_{\nu,q}|C_k|}{|C_k|} + \frac{i}{\hbar}\partial_{\nu,q}S_k \right) \left( \frac{\partial_{\mu,p}|C_k|}{|C_k|} + \frac{i}{\hbar}\partial_{\mu,p}S_k \right) \left( \frac{\partial_{\mu,p}|C_l|}{|C_l|} - \frac{i}{\hbar}\partial_{\mu,p}S_l \right) |C_k|^2 |C_l|^2 \right\} \right] \\ &= -\sum_{\mu,p} \frac{\hbar^2}{2M_\mu} \left[ \sum_k 2\Re \left\{ \left[ \partial_{\nu,q} \left( \frac{\partial_{\mu,p}|C_k|}{|C_k|} - \frac{i}{\hbar}\partial_{\mu,p}S_k \right) \right] \left( \frac{\partial_{\mu,p}|C_k|}{|C_k|} + \frac{i}{\hbar}\partial_{\mu,p}S_k \right) |C_k|^2 \right. \right. \\ &\quad \left. \left. + \left( \frac{\partial_{\nu,q}|C_k|}{|C_k|} - \frac{i}{\hbar}\partial_{\nu,q}S_k \right) \left( \left( \frac{\partial_{\mu,p}|C_k|}{|C_k|} \right)^2 + \frac{1}{\hbar^2}(\partial_{\mu,p}S_k)^2 \right) |C_k|^2 \right\} \right. \\ &\quad \left. - \sum_{k,l} 2\Re \left\{ \left( \frac{\partial_{\nu,q}|C_k|}{|C_k|} - \frac{i}{\hbar}\partial_{\nu,q}S_k \right) \left( \frac{\partial_{\mu,p}|C_k|}{|C_k|} + \frac{i}{\hbar}\partial_{\mu,p}S_k \right) \left( -\frac{i}{\hbar}\partial_{\mu,p}S_l \right) |C_k|^2 |C_l|^2 \right. \right. \\ &\quad \left. \left. + \left[ \partial_{\nu,q} \left( \frac{\partial_{\mu,p}|C_k|}{|C_k|} + \frac{i}{\hbar}\partial_{\mu,p}S_k \right) \right] \left( -\frac{i}{\hbar}\partial_{\mu,p}S_l \right) |C_k|^2 |C_l|^2 \right. \right. \\ &\quad \left. \left. + \left( \frac{\partial_{\nu,q}|C_k|}{|C_k|} + \frac{i}{\hbar}\partial_{\nu,q}S_k \right) \left( \frac{\partial_{\mu,p}|C_k|}{|C_k|} + \frac{i}{\hbar}\partial_{\mu,p}S_k \right) \left( -\frac{i}{\hbar}\partial_{\mu,p}S_l \right) |C_k|^2 |C_l|^2 \right\} \right],\end{aligned}\tag{S14}$$

where terms that goes to zero when expanded and summed over  $l$  are removed.

If we collect the real part, we get

$$\begin{aligned}
F_{\nu,q}^{\text{GI}} &= - \sum_{\mu,p} \frac{\hbar^2}{M_\mu} \left[ \sum_k \left\{ \partial_{\nu,q} \left( \frac{\partial_{\mu,p}|C_k|}{|C_k|} \right) \frac{\partial_{\mu,p}|C_k|}{|C_k|} + \frac{1}{\hbar^2} \partial_{\nu,q} \partial_{\mu,p} S_k \partial_{\mu,p} S_k \right. \right. \\
&\quad \left. \left. + \frac{\partial_{\nu,q}|C_k|}{|C_k|} \left( \frac{\partial_{\mu,p}|C_k|}{|C_k|} \right)^2 + \frac{\partial_{\nu,q}|C_k|}{|C_k|} \frac{1}{\hbar^2} (\partial_{\mu,p} S_k)^2 \right\} |C_k|^2 \right. \\
&\quad \left. - \sum_{k,l} \left\{ \frac{\partial_{\nu,q}|C_k|}{|C_k|} \frac{1}{\hbar^2} \partial_{\mu,p} S_k \partial_{\mu,p} S_l - \frac{1}{\hbar^2} \partial_{\nu,q} S_k \frac{\partial_{\mu,p}|C_k|}{|C_k|} \partial_{\mu,p} S_l \right. \right. \\
&\quad \left. \left. + \frac{1}{\hbar^2} \partial_{\nu,q} \partial_{\mu,p} S_k \partial_{\mu,p} S_l \right. \right. \\
&\quad \left. \left. + \frac{\partial_{\nu,q}|C_k|}{|C_k|} \frac{1}{\hbar^2} \partial_{\mu,p} S_k \partial_{\mu,p} S_l + \frac{1}{\hbar^2} \partial_{\nu,q} S_k \frac{\partial_{\mu,p}|C_k|}{|C_k|} \partial_{\mu,p} S_l \right\} |C_k|^2 |C_l|^2 \right] \\
&= - \sum_{\mu,p} \frac{\hbar^2}{M_\mu} \left[ \sum_{k,l} \left\{ \partial_{\nu,q} \left( \frac{\partial_{\mu,p}|C_k|}{|C_k|} \right) \frac{\partial_{\mu,p}|C_k|}{|C_k|} + \frac{\partial_{\nu,q}|C_k|}{|C_k|} \left( \frac{\partial_{\mu,p}|C_k|}{|C_k|} \right)^2 \right. \right. \\
&\quad \left. \left. + \frac{1}{\hbar^2} \partial_{\nu,q} \partial_{\mu,p} S_k (\partial_{\mu,p} S_k - \partial_{\mu,p} S_l) \right. \right. \\
&\quad \left. \left. + \frac{\partial_{\nu,q}|C_k|}{|C_k|} \frac{1}{\hbar^2} \partial_{\mu,p} S_k (\partial_{\mu,p} S_k - 2\partial_{\mu,p} S_l) \right\} |C_k|^2 |C_l|^2 \right] \tag{S15} \\
&= - \sum_{\mu,p} \frac{\hbar^2}{M_\mu} \left[ \sum_{k,l} \left\{ \partial_{\nu,q} \left( \frac{\partial_{\mu,p}|C_k|}{|C_k|} \right) \frac{\partial_{\mu,p}|C_k|}{|C_k|} + \frac{\partial_{\nu,q}|C_k|}{|C_k|} \left( \frac{\partial_{\mu,p}|C_k|}{|C_k|} \right)^2 \right. \right. \\
&\quad \left. \left. + \frac{1}{\hbar^2} \partial_{\nu,q} \partial_{\mu,p} S_k (\partial_{\mu,p} S_k - \partial_{\mu,p} S_l) \right. \right. \\
&\quad \left. \left. + \frac{\partial_{\nu,q}|C_k|}{|C_k|} \frac{1}{\hbar^2} ((\partial_{\mu,p} S_k)^2 - 2\partial_{\mu,p} S_k \partial_{\mu,p} S_l) \right. \right. \\
&\quad \left. \left. + \frac{\partial_{\nu,q}|C_k|}{|C_k|} \frac{1}{\hbar^2} (\partial_{\mu,p} S_l)^2 \right\} |C_k|^2 |C_l|^2 \right] \\
&= - \sum_{\mu,p} \frac{\hbar^2}{M_\mu} \left[ \sum_{k,l} \left\{ \partial_{\nu,q} \left( \frac{\partial_{\mu,p}|C_k|}{|C_k|} \right) \frac{\partial_{\mu,p}|C_k|}{|C_k|} + \frac{\partial_{\nu,q}|C_k|}{|C_k|} \left( \frac{\partial_{\mu,p}|C_k|}{|C_k|} \right)^2 \right. \right. \\
&\quad \left. \left. + \frac{1}{\hbar^2} \partial_{\nu,q} \partial_{\mu,p} S_k (\partial_{\mu,p} S_k - \partial_{\mu,p} S_l) \right. \right. \\
&\quad \left. \left. + \frac{\partial_{\nu,q}|C_k|}{|C_k|} \frac{1}{\hbar^2} (\partial_{\mu,p} S_k - \partial_{\mu,p} S_l)^2 \right\} |C_k|^2 |C_l|^2 \right],
\end{aligned}$$

where we added a term that goes to zero to symmetrize the equation. Neglecting  $O(\hbar^2)$  terms, we get

$$\begin{aligned}
F_{\nu,q}^{\text{GI}} &= - \sum_{\mu} \frac{\hbar^2}{M_\mu} \left[ \sum_{k,l} \left\{ \frac{1}{\hbar^2} \sum_p \partial_{\nu,q} \partial_{\mu,p} S_k (\partial_{\mu,p} S_k - \partial_{\mu,p} S_l) \right. \right. \\
&\quad \left. \left. + \frac{\partial_{\nu,q}|C_k|}{|C_k|} \frac{1}{\hbar^2} (\partial_{\mu,p} S_k - \partial_{\mu,p} S_l)^2 \right\} |C_k|^2 |C_l|^2 \right] \tag{S16}
\end{aligned}$$

As a result, we can write  $\mathbf{F}_\nu^{\text{GI}}$  in terms of matrix multiplication:

$$\begin{aligned}
\mathbf{F}_\nu^{\text{GI}} &= - \sum_{k,l} \sum_{\mu} \left( \frac{\mathbf{H}_{\nu\mu,kl} \mathbf{D}_{\mu,kl}}{2M_\mu} \right) |C_k|^2 |C_l|^2 \\
&\quad - \sum_{k,l} \frac{\nabla_\nu |C_k|}{|C_k|} \left( \sum_{\mu} \frac{|\mathbf{D}_{\mu,kl}|^2}{M_\mu} \right) |C_k|^2 |C_l|^2, \tag{S17}
\end{aligned}$$

where  $\mathbf{H}_{\nu\mu,kl}$  is a  $3 \times 3$  sub-Hessian matrix of phase difference for nucleus  $\nu$  and  $\mu$ , i.e.  $[\mathbf{H}_{\nu\mu,kl}]_{pq} = \partial_{\nu p} \partial_{\mu q} (S_k - S_l)$ .

Finally, if we substitute above for  $\mathbf{F}_\nu^{\text{GI}}$  we get the nuclear force in terms of BO representation as:

$$\begin{aligned} \mathbf{F}_\nu = & - \sum_k |C_k|^2 \nabla_\nu \epsilon_k - \sum_{k,l} C_k C_l^* (\epsilon_k - \epsilon_l) \mathbf{d}_{\nu,kl} \\ & - \sum_{k,l} \mathbf{D}_{\nu,kl} \left\{ \sum_\mu \frac{1}{2M_\mu} (\mathcal{P}_\mu + \mathcal{Q}_{\mu,kl} + \nabla_\mu) \cdot \mathbf{D}_{\mu,kl} \right\} |C_l|^2 |C_k|^2 \\ & - \sum_{k,l} \sum_\mu \left( \frac{\mathbf{H}_{\nu\mu,kl} \mathbf{D}_{\mu,kl}}{2M_\mu} \right) |C_k|^2 |C_l|^2, \end{aligned} \quad (\text{S18})$$

where  $\mathbf{F}_\nu^{\text{Ph}}$  is canceled by a component of  $\mathbf{F}_\nu^{\text{GI}}$ .

### C. Numerical implementation

We now introduce the numerical implementation of the new exact mixed quantum-classical equations derived in this work. The reduced PQM  $\mathcal{Q}_{\nu,jk}$  can be calculated using the "bare" PQM:  $\mathcal{G}_{\nu,jk} = \nabla_\nu |\chi_j|^2 / |\chi_j|^2 + \nabla_\nu |\chi_k|^2 / |\chi_k|^2 = \mathcal{Q}_{\nu,jk} + 2\mathcal{P}_\nu$ , where  $\chi_i = C_i \chi$  is the BO projected nuclear wave function. Therefore, we first define the BO projected nuclear density for each state as a multi-dimensional Gaussian function based on the nuclear configurations and BO populations of trajectories [2] as

$$|\chi_j(\underline{\mathbf{R}}, t)|^2 \equiv \frac{\langle |C_j|^2 \rangle(t)}{\mathcal{N}_j(t)} \prod_\nu \exp \left( -\frac{|\mathbf{R}_\nu - \mathbf{R}_{\nu,j}(t)|^2}{2\sigma_{\nu,j}(t)^2} \right), \quad (\text{S19})$$

where  $\mathcal{N}_i$  is the normalization factor. The Gaussian center and variance for each state are then defined as follows:

$$\begin{aligned} \mathbf{R}_{\nu,j}(t) & \equiv \frac{\sum_I^{N_{\text{traj}}} |C_j^{(I)}(t)|^2 \mathbf{R}_\nu^{(I)}(t)}{N_{\text{traj}} \langle |C_j|^2 \rangle(t)} \\ & = \frac{\sum_I^{N_{\text{traj}}} |C_j^{(I)}(t)|^2 \mathbf{R}_\nu^{(I)}(t)}{\sum_J^{N_{\text{traj}}} |C_j^{(J)}(t)|^2}, \end{aligned} \quad (\text{S20})$$

$$\sigma_{\nu,j}(t)^2 \equiv \frac{\sum_I^{N_{\text{traj}}} |C_j^{(I)}(t)|^2 |\mathbf{R}_\nu^{(I)}(t) - \mathbf{R}_{\nu,j}(t)|^2}{\sum_J^{N_{\text{traj}}} |C_j^{(J)}(t)|^2}, \quad (\text{S21})$$

with  $N_{\text{traj}}$  denoting the number of trajectories. Then, the total quantum momentum  $\mathcal{P}_\nu$  can be calculated from the total nuclear density, defined as the sum of the BO projected nuclear densities in the XF formalism:  $|\chi(\underline{\mathbf{R}}, t)|^2 = \sum_k |\chi_k(\underline{\mathbf{R}}, t)|^2$ . As a result, we get

$$\mathcal{G}_{\nu,jk}^{(I)} = - \left[ \left( \frac{1}{\sigma_{\nu,j}^2} + \frac{1}{\sigma_{\nu,k}^2} \right) \mathbf{R}_\nu^{(I)} - \left( \frac{\mathbf{R}_{\nu,j}}{\sigma_{\nu,j}^2} + \frac{\mathbf{R}_{\nu,k}}{\sigma_{\nu,k}^2} \right) \right] \quad (\text{S22})$$

and

$$\mathcal{P}_\nu^{(I)} = - \left[ \sum_l \left( \frac{|C_l^{(I)}|^2}{\sigma_{\nu,l}^2} \right) \mathbf{R}_\nu^{(I)} - \sum_l \left( \frac{|C_l^{(I)}|^2 \mathbf{R}_{\nu,l}}{\sigma_{\nu,l}^2} \right) \right]. \quad (\text{S23})$$

The second derivative terms  $\mathbf{H}_{\nu\mu,kl}$  and  $\nabla_\nu \cdot \mathbf{D}_{\nu,kl}$  can be approximated as time-integral of Hessian matrix elements of BO potential energy. However, it would make simulations more computationally expensive. Instead, we introduce  $\Delta_{\nu,jk}$  to replace  $\nabla_\nu \cdot \mathbf{D}_{\nu,jk}$  and ensure the averaged BO population conservation in the absence of NAC and the vanishing  $\nabla_\nu S_j$  at  $\underline{\mathbf{R}} \rightarrow \infty$  condition for exact dynamics. From the averaged BO population conservation condition:

$$\sum_I \frac{d}{dt} |C_j^{(I)}|^2 = - \sum_I \sum_\nu \frac{1}{M_\nu} \sum_k \left\{ \left( \mathcal{Q}_{\nu,jk}^{(I)} + \mathcal{P}_{\nu,jk}^{(I)} \right) \cdot \mathbf{D}_{\nu,jk}^{(I)} + \Delta_{\nu,jk} \right\} |C_k^{(I)}|^2 |C_j^{(I)}|^2 = 0, \quad (\text{S24})$$

we define a uniform pair-wise shift term  $\Delta_{\nu,ik}$  for each nucleus as

$$\Delta_{\nu,jk} = -\frac{\sum_I \left\{ \left( \mathcal{Q}_{\nu,jk}^{(I)} + \mathcal{P}_{\nu,jk}^{(I)} \right) \cdot \mathbf{D}_{\nu,jk}^{(I)} \right\} |C_k^{(I)}|^2 |C_j^{(I)}|^2}{\sum_J |C_k^{(J)}|^2 |C_j^{(J)}|^2}. \quad (\text{S25})$$

Meanwhile,  $\nabla_\nu S_j^{(I)}$ , which previously named as “phase term”, can be approximated in different ways [2–5]. In this work, we approximate  $\nabla_\nu S_j^{(I)}$  to a BO momentum  $\mathbf{P}_{\nu,j}^{(I)} \equiv \alpha_j^{(I)} \mathbf{P}_\nu^{(I)}$  which can be calculated based on the total energy conservation condition introduced in the main text where we used  $E_{\text{tot}}^{(I)}(t=0)$  in this work to use a constant value for stability. Finally, dropping the terms merely contribute to the global phase, the working MQC equations for the new CTMQC method are obtained as follows:

$$\begin{aligned} \dot{C}_j^{(I)} = & -\frac{i}{\hbar} \epsilon_j^{(I)} C_j^{(I)} - \sum_k \sum_\nu \frac{\mathbf{P}_\nu^{(I)}}{M_\nu} \cdot \mathbf{d}_{\nu,jk}^{(I)} C_k^{(I)} \\ & - \sum_\nu \sum_k \left\{ \frac{\mathcal{G}_{\nu,jk}^{(I)} - \mathcal{P}_\nu^{(I)}}{2M_\nu} \cdot \mathbf{D}_{\nu,jk}^{(I)} + \Delta_{\nu,jk} \right\} |C_k^{(I)}|^2 C_j^{(I)} \\ & - \frac{i}{\hbar} \left( \sum_\nu \frac{|\mathbf{P}_{\nu,j}^{(I)}|^2}{2M_\nu} - \frac{\mathbf{P}_{\nu,j}^{(I)} \cdot \mathbf{P}_\nu^{(I)}}{M_\nu} \right) C_j^{(I)}, \end{aligned} \quad (\text{S26})$$

and

$$\begin{aligned} \mathbf{F}_\nu^{(I)} = & -\sum_k |C_k^{(I)}|^2 \nabla_\nu \epsilon_k^{(I)} - \sum_{k,l} C_k^{(I)} C_l^{(I)*} (\epsilon_k - \epsilon_l)^{(I)} \mathbf{d}_{\nu,lk}^{(I)} \\ & - \sum_{k,l} \mathbf{D}_{\nu,kl}^{(I)} \left\{ \sum_\mu \frac{\mathcal{G}_{\mu,kl}^{(I)} - \mathcal{P}_\mu^{(I)}}{2M_\mu} \cdot \mathbf{D}_{\mu,kl}^{(I)} + \Delta_{\nu,lk} \right\} |C_l^{(I)}|^2 |C_k^{(I)}|^2. \end{aligned} \quad (\text{S27})$$

Compared to the original coupled trajectory MQC (CTMQC) equations, the total quantum momentum is changed to an "effective" quantum momentum  $\mathcal{G}_{\nu,jk} - \mathcal{P}_\nu$  for each pair of states, and the phase correction term and  $\Delta_{\nu,jk}$  term are added.

The new CTMQC simulations can be performed by following the steps below. First, we select a set of nuclear configurations and momenta using an appropriate sampling method (e.g. Wigner or Boltzmann sampling), along with the initial BO state that each trajectory occupies. For each trajectory, a static calculation of BO potential energies, their gradients, and NACs is performed at the corresponding nuclear position. Then, we compute  $\mathbf{D}_{\nu,lk}$  from the total energy and the current momentum of each trajectory. Next, using the information from all trajectories, we calculate the QM and PQM for each trajectory, and calculate  $\Delta_{\nu,lk}$ . We then evaluate the nuclear force and the time derivative of the BO coefficients according to Eqs. (S27) and (S26), respectively, for each nuclear trajectory, so that we propagate the nuclear trajectory and corresponding electronic state. This procedure is repeated from the static calculation step until the end of the simulation.

In the surface hopping based on exact factorization (SHXF) method, while the nuclear force and the hopping algorithm follow the conventional surface hopping (SH) scheme [6], PQM can be readily incorporated with negligible additional computational cost, as we can directly exploit the already-defined BO-projected nuclear density from the auxiliary trajectory on each state  $\mathbf{R}_{\nu,i} = \mathbf{R}_{\nu,i}^{(I)}$  [4, 7]. The variance  $\sigma_\nu^2$  is set identical for all states. As a result,

$$\mathcal{G}_{\nu,ik}^{(I)} = -\frac{2\mathbf{R}_\nu^{(I)} - \mathbf{R}_{\nu,i}^{(I)} - \mathbf{R}_{\nu,k}^{(I)}}{\sigma_\nu^2} \quad (\text{S28})$$

and

$$\mathcal{P}_\nu^{(I)} = -\frac{\mathbf{R}_\nu^{(I)} - \sum_k \left( |C_k^{(I)}|^2 \mathbf{R}_{\nu,k}^{(I)} \right)}{\sigma_\nu^2}. \quad (\text{S29})$$

The phase correction term in the SHXF method becomes identical to the phase-corrected SH (PCSH) method [8] if we use  $\nabla_\nu S_j \equiv \mathbf{P}_j$ .

## II. COMPUTATIONAL DETAIL

The molecular Hamiltonian for two-state model systems can be expressed as

$$\hat{H}(\underline{\mathbf{R}}) = \hat{T}_n(\underline{\mathbf{R}}) + \hat{H}_{BO}(\underline{\mathbf{R}}), \quad (\text{S30})$$

where  $\hat{T}_n$  and  $\hat{H}_{BO}$  are the nuclear kinetic energy and the BO Hamiltonian operators, respectively. The BO Hamiltonian matrix in the diabatic basis is

$$\hat{H}_{BO} = \begin{pmatrix} V_{11}(\underline{\mathbf{R}}) & V_{12}(\underline{\mathbf{R}}) \\ V_{21}(\underline{\mathbf{R}}) & V_{22}(\underline{\mathbf{R}}) \end{pmatrix}, \quad (\text{S31})$$

where  $V_{ij}$  is defined for each model.

For both the double arch geometry (DAG) and two-dimensional non-separable (2DNS) models, the exact quantum wave-packet dynamics is performed using the split-operator technique [9] on a spatial grid for the nuclear degrees of freedom, with a time step of 0.1 a.u. A time step of 1.0 a.u. is used for the MQC simulations in both models. The mass of the nuclear degrees of freedom is set to 2000.0 a.u. For SH-based dynamics simulations, we use 1000 trajectories, whereas the CT methods propagate 200 trajectories.

The standard deviation parameter for SHXF simulations is set to the same value as that of the initial nuclear density while the EDC and EDC2 parameters are taken from Refs. 10 and 11, respectively.

The energy-based correction (EDC) scheme [10, 12] for SH methods rescales the BO coefficients of each trajectory with the decoherence time constant  $\tau_{ja}$  at every time step as

$$C'_j = C_j \exp(-\Delta t / \tau_{ja}) \quad (\text{S32})$$

$$C'_a = C_a \sqrt{\frac{1 - \sum_{j \neq a} |C'_j|^2}{|C_a|^2}}, \quad (\text{S33})$$

where  $a$  is the active state of the trajectory, so that the electronic state of the trajectory decoheres toward the active state.

The time constant for PCSH-EDC is defined [10] as

$$\tau_{ja} = \frac{1}{|\epsilon_j - \epsilon_a|} \left( 1 + \frac{C}{E_{\text{kin}}} \right), \quad (\text{S34})$$

where  $C = 0.1$  a.u. and  $E_{\text{kin}}$  is the kinetic energy of a trajectory, while PCSH-EDC2 employs

$$\tau_{ja} = C_0 + C_1 \frac{\max(E_{\text{kin}}, \epsilon_j - \epsilon_a)}{E_{\text{kin}} - (\epsilon_j - \epsilon_a)}, \quad (\text{S35})$$

where  $C_0 = 2.5 \times 10^{-3}$  and  $C_1 = 2.0^5$ , which was proposed by Shao and coworkers in Ref. 12.

### A. Double arch geometry model

The diabatic Hamiltonian matrix elements of the DAG model are given by

$$V_{11}(R) = a, \quad (\text{S36})$$

$$V_{22}(R) = -a, \quad (\text{S37})$$

$$V_{12}(R) = V_{21}(R) = \begin{cases} -b \exp(c(R-d)) + b \exp(c(R+d)) & \text{if } R < -d, \\ -b \exp(c(R-d)) - b \exp(-c(R+d)) + 2b & \text{if } -d \leq R \leq d, \\ b \exp(-c(R-d)) - b \exp(-c(R+d)) & \text{if } R > d \end{cases}, \quad (\text{S38})$$

where  $a = 6 \times 10^{-4}$ ,  $b = 0.1$ ,  $c = 0.9$ , and  $d = 4.0$ .

The initial molecular wave function is set to a nuclear Gaussian function centered at  $R_0 = -25.0$  a.u. on the lower BO state with a momentum delta-kick  $k_0$  with the standard deviation  $\sigma = 2.0$  a.u., i.e.

$$|\Psi(R, t_0)\rangle = \mathcal{N} \exp\left(-\frac{(R - R_0)^2}{4\sigma^2}\right) \exp(ik_0(R - R_0)) |\phi_1\rangle. \quad (\text{S39})$$

The initial conditions of the nuclear trajectories are obtained from the Wigner sampling of the above wave function, and the initial BO coefficient for the lower state is set to 1.0.

### B. Two-dimensional non-separable model

The diabatic Hamiltonian matrix elements of the 2DNS model are given by

$$V_{11}(x, y) = -E_0, \quad (S40)$$

$$V_{22}(x, y) = -A \exp(-B(0.75(x+y)^2 + 0.25(x-y)^2)), \quad (S41)$$

$$V_{12}(x, y) = V_{21}(x, y) = C \exp(-D(0.25(x+y)^2 + 0.75(x-y)^2)), \quad (S42)$$

where  $A = 0.15$ ,  $B = 0.14$ ,  $C = 0.015$ ,  $D = 0.06$ , and  $E_0 = 0.05$  a.u.

Similar to the DAG model simulations, the initial molecular wave function is set to a two-dimensional nuclear Gaussian function centered at  $(x_0, y_0) = (-8.0, 0.0)$  a.u. on the lower BO state with a momentum delta-kick  $(k_{0x}, k_{0y}) = (k_0, 0.0)$  a.u. with the standard deviation  $(\sigma_x, \sigma_y) = (0.5, 0.5)$  a.u., i.e.

$$|\Psi(x, y, t_0)\rangle = \mathcal{N} \exp\left(-\frac{(x-x_0)^2}{4\sigma_x^2}\right) \exp\left(-\frac{y^2}{4\sigma_y^2}\right) \exp(ik_0(x-x_0)) |\phi_1\rangle, \quad (S43)$$

and the trajectories are generated correspondingly with the Wigner sampling.

### III. SUPPLEMENTARY RESULTS

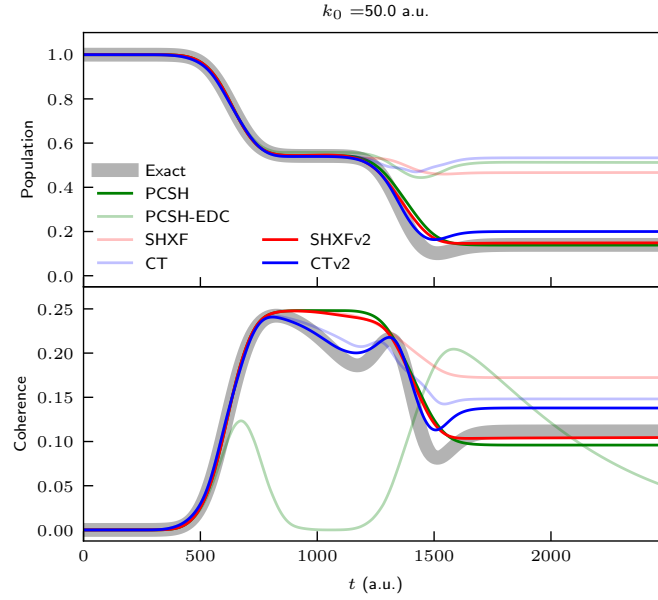


FIG. S1: Time evolution of BO population  $\langle |C_1|^2 \rangle(t)$  (upper) and coherence  $\langle |C_1 C_2|^2 \rangle(t)$  (lower) with initial momentum  $k_0 = 50$  a.u.



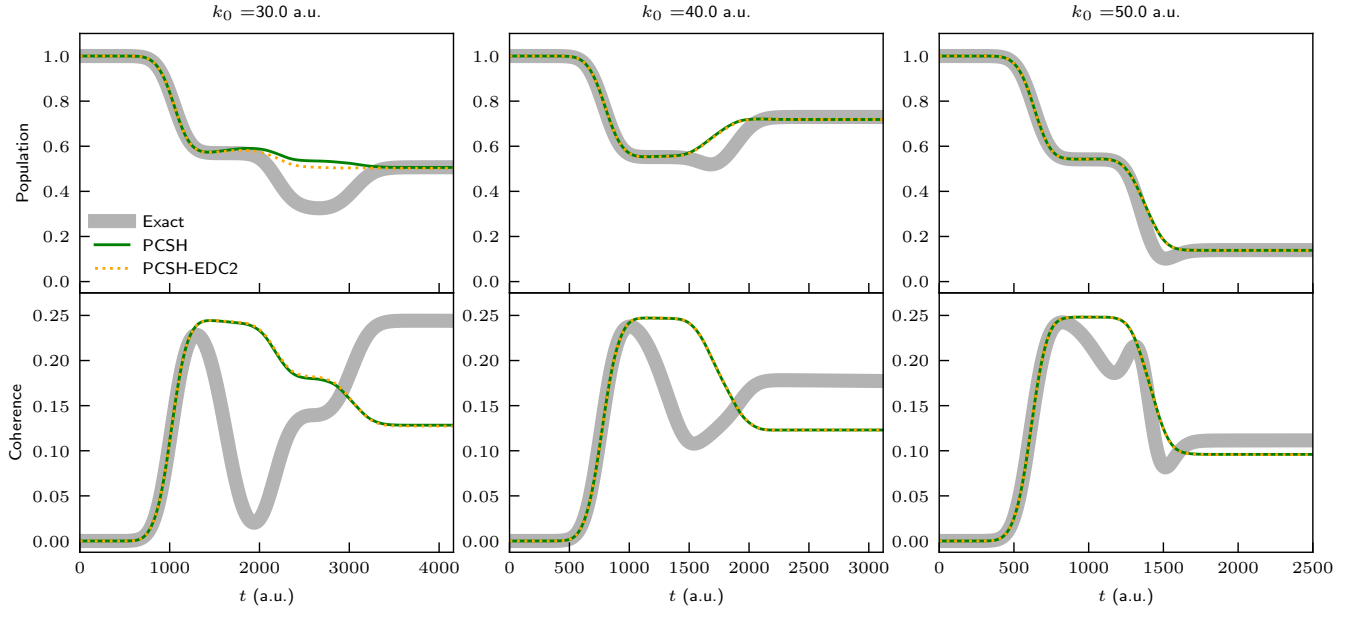


FIG. S2: Time evolution of BO population  $\langle |C_1|^2 \rangle(t)$  (upper) and coherence  $\langle |C_1 C_2|^2 \rangle(t)$  (lower) with different initial momenta  $k_0 = 30, 40$  and  $50$  a.u. for PCSH-EDC2.

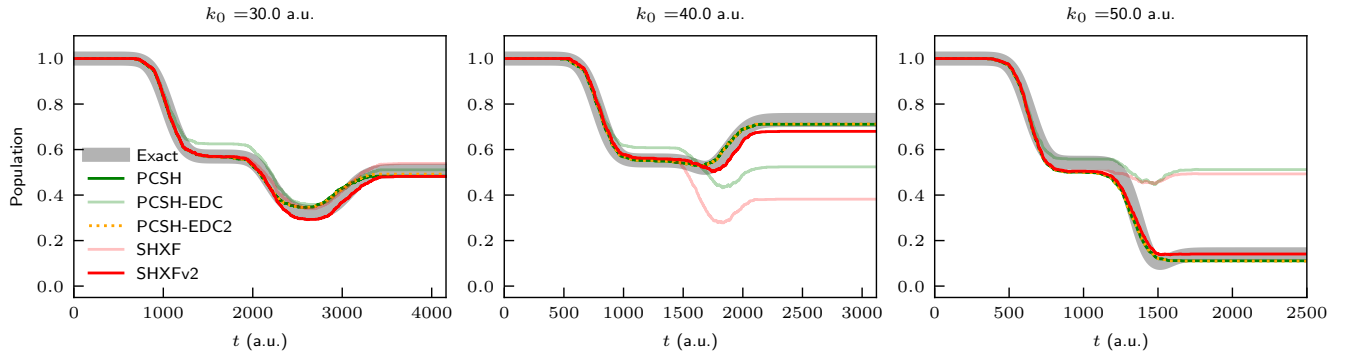


FIG. S3: Time evolution of BO population calculated based on the active state  $a^{(I)}(t)$  of trajectories:  $P_i(t) = \sum_I \delta_{ia^{(I)}(t)} / N_{\text{traj}}$ , with different initial momenta  $k_0 = 30, 40$  and  $50$  a.u. for SH-based methods.

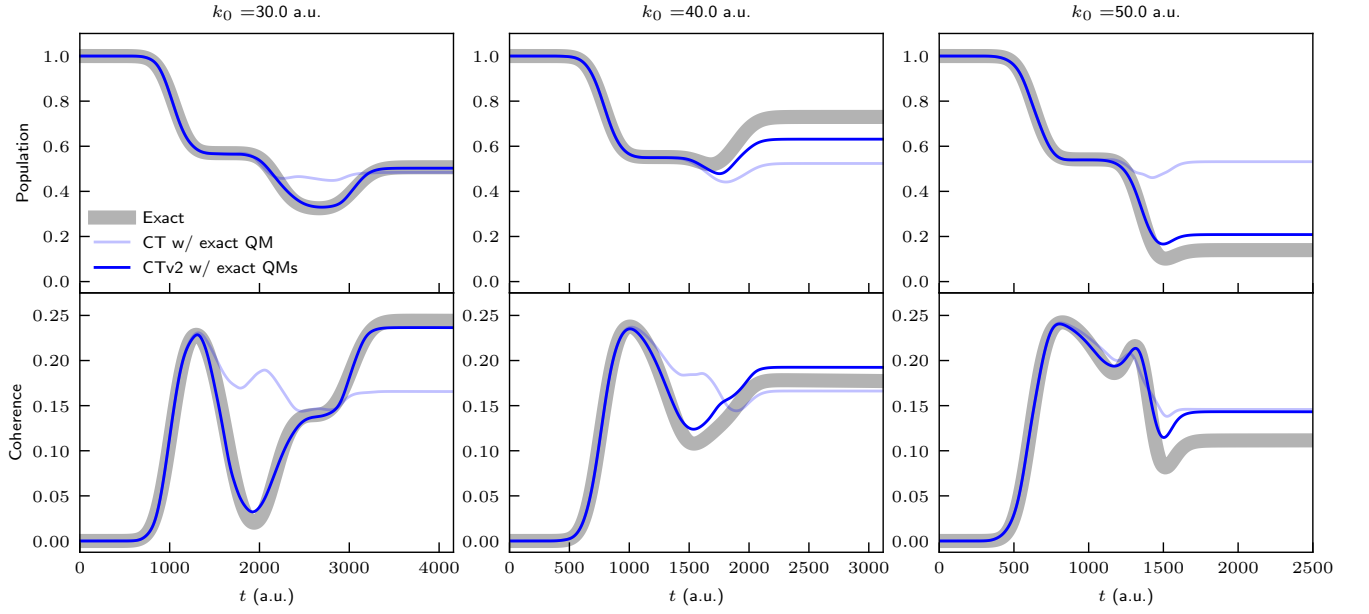


FIG. S4: Time evolution of BO population  $\langle |C_1|^2 \rangle(t)$  (upper) and coherence  $\langle |C_1 C_2|^2 \rangle(t)$  (lower) with different initial momenta  $k_0 = 30, 40$  and  $50$  a.u. for CT methods with the QM  $\mathcal{P}_\nu$  (and PQM,  $\mathcal{Q}_{\nu,ik}$  for CTv2) obtained from quantum dynamics.

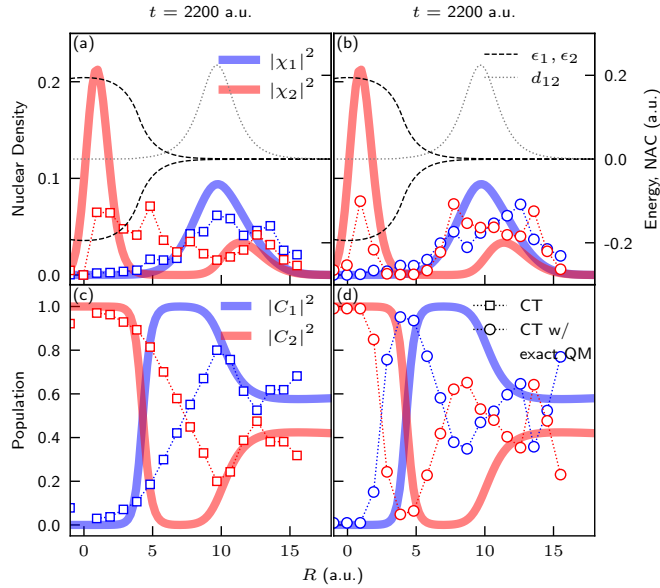


FIG. S5: Spatial distribution of nuclear wave packets (a,b) and BO populations (c,d) at  $t = 2200$  a.u. with the initial momentum  $k_0 = 30.0$  a.u. for CT (a,c) and CT with the QM,  $\mathcal{P}_\nu$ , obtained from quantum dynamics (b,d). The BO potential energies  $\epsilon_{1/2}$  and the NAC  $d_{12}$  are depicted to interpret wave packet dynamics (a,b).

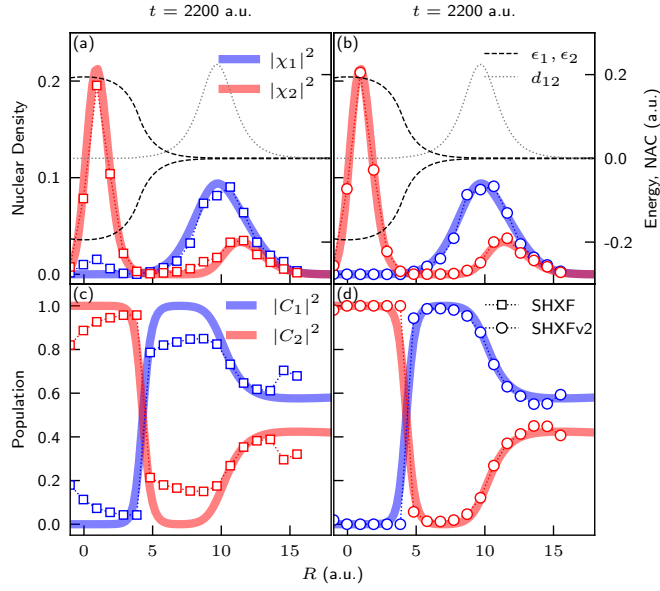


FIG. S6: Spatial distribution of nuclear wave packets (a,b) and BO populations (c,d) at  $t = 2200$  a.u. with the initial momentum  $k_0 = 30.0$  a.u. for SHXF (a,c) and SHXFv2 (b,d) methods. BO potentials and NAC are depicted as in Fig. S5.

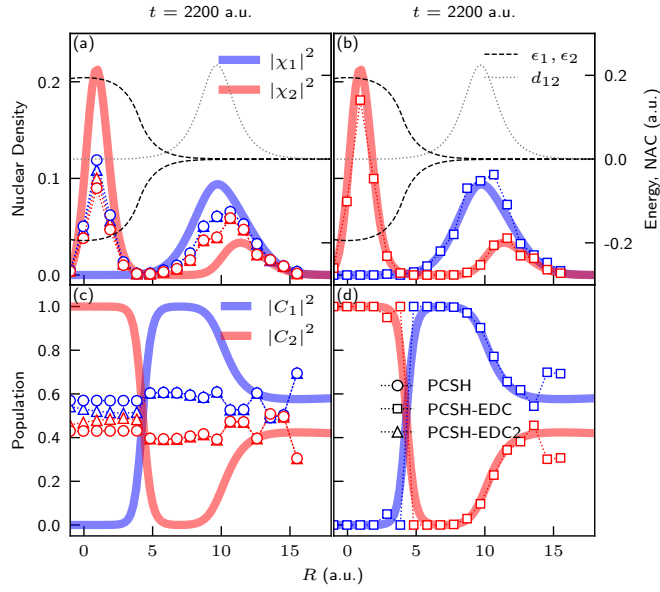


FIG. S7: Spatial distribution of nuclear wave packets (a,b) and BO populations (c,d) at  $t = 2200$  a.u. with the initial momentum  $k_0 = 30.0$  a.u. for PCSH, PCSH-EDC2 (a,c), and PCSH-EDC (b,d). BO potentials and NAC are depicted as in Fig. S5.

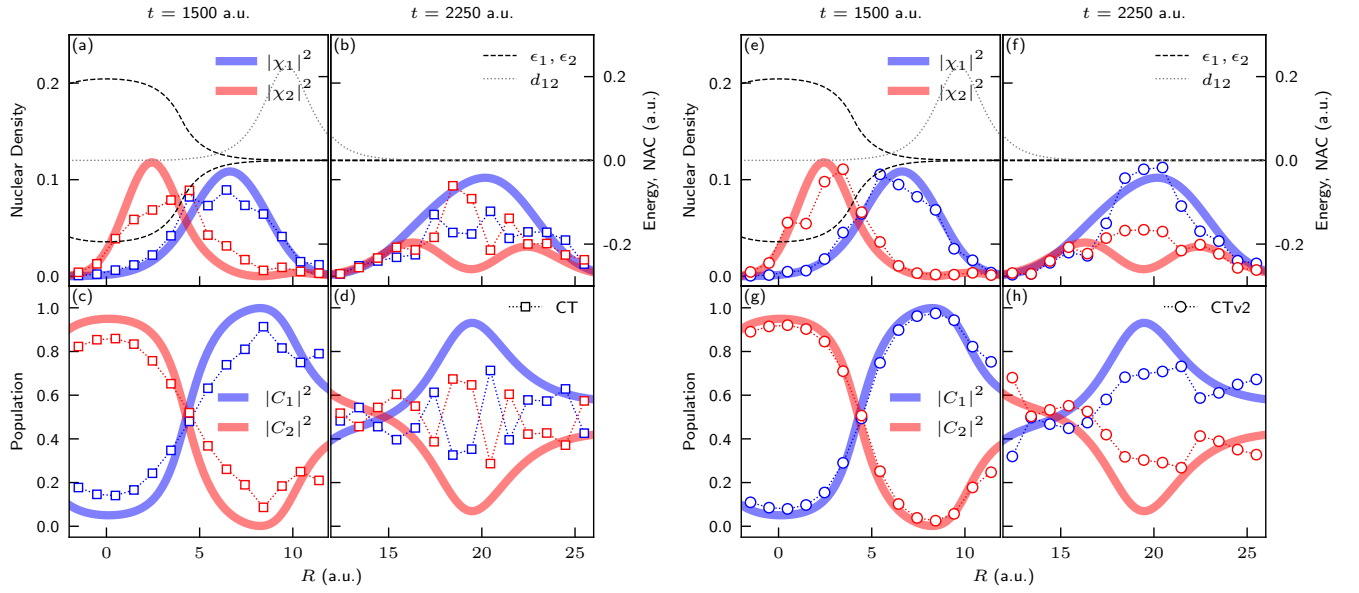


FIG. S8: Spatial distribution of nuclear wave packets and BO populations at different time steps,  $t = 1500$  a.u. (a,c,e,g) and 2250 a.u. (b,d,f,h) with the initial momentum  $k_0 = 40.0$  a.u. for CT (a-d) and CT2 (e-h). BO potentials and NAC are depicted as in Fig. S5.

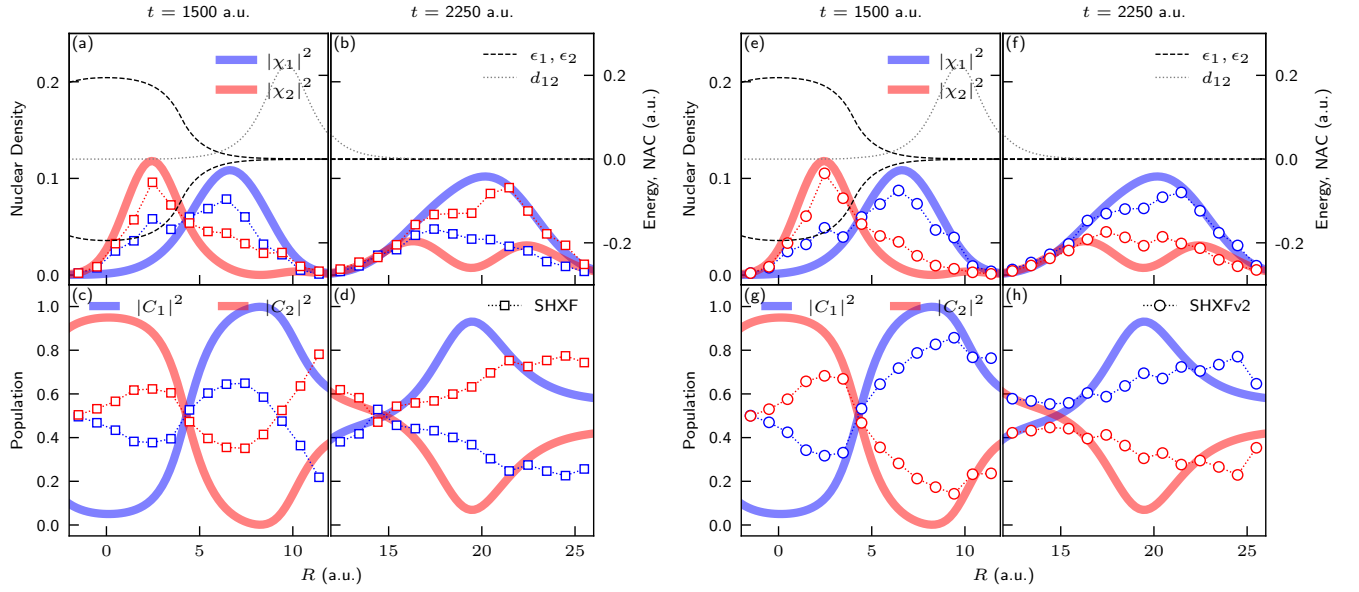


FIG. S9: Spatial distribution of nuclear wave packets and BO populations at different time steps,  $t = 1500$  a.u. (a,c,e,g) and 2250 a.u. (b,d,f,h) with the initial momentum  $k_0 = 40.0$  a.u. for SHXF (a-d) and SHXF2 (e-h). BO potentials and NAC are depicted as in Fig. S5.

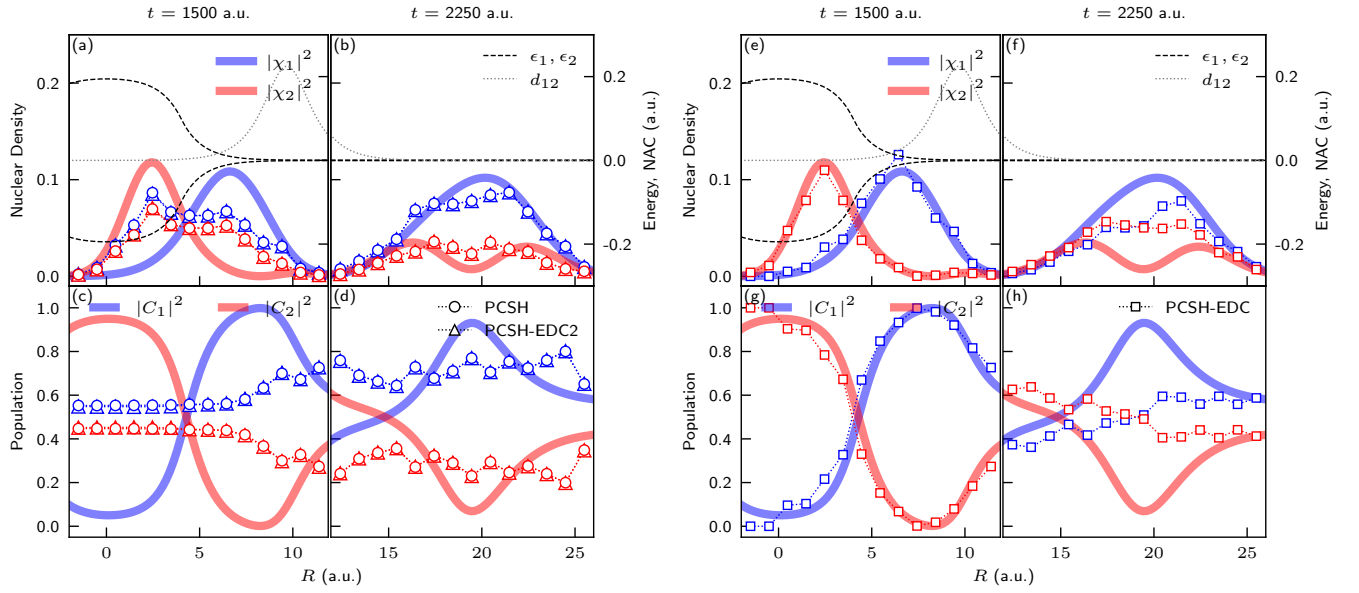


FIG. S10: Spatial distribution of nuclear wave packets and BO populations at different time steps,  $t = 1500$  a.u. (a,c,e,g) and 2250 a.u. (b,d,f,h) with the initial momentum  $k_0 = 40.0$  a.u. for PCSH, PCSH-EDC2 (a-d), and PCSH-EDC (e-h). BO potentials and NAC are depicted as in Fig. S5.

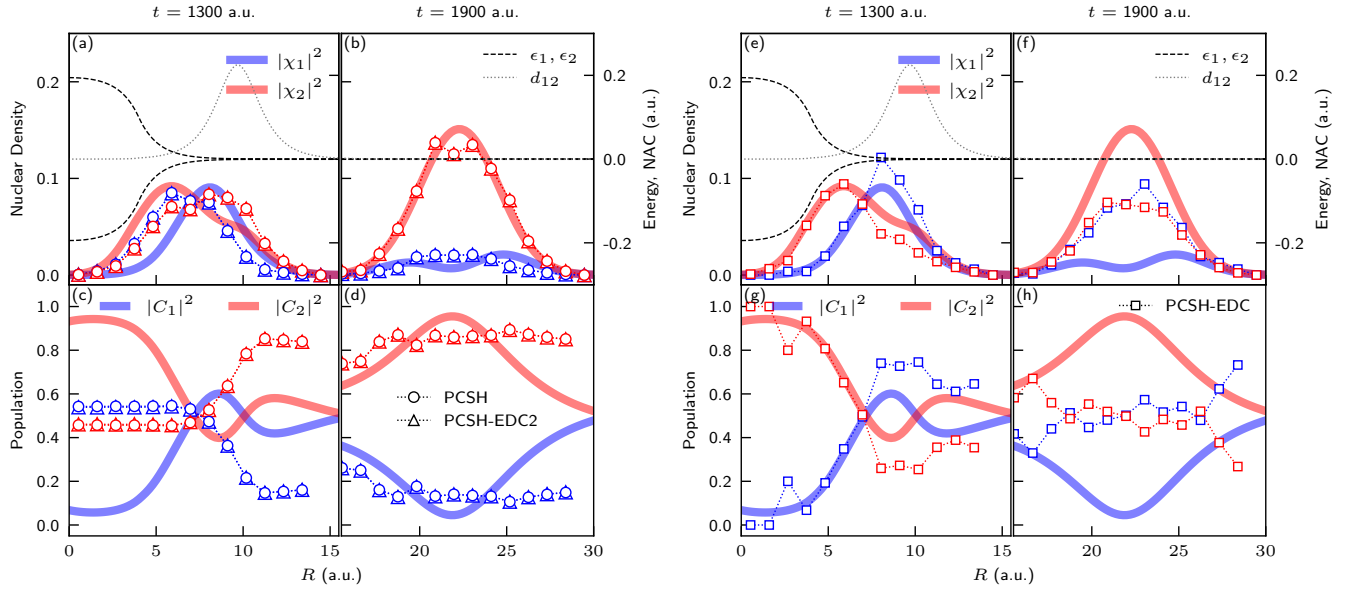


FIG. S11: Spatial distribution of nuclear wave packets and BO populations at different time steps,  $t = 1300$  a.u. (a,c,e,g) and 1900 a.u. (b,d,f,h) with the initial momentum  $k_0 = 50.0$  a.u. for PCSH, PCSH-EDC2 (a-d), and PCSH-EDC (e-h). BO potentials and NAC are depicted as in Fig. S5.

- 
- [1] E. V. Arribas and N. T. Maitra, Electronic Coherences in Molecules: The Projected Nuclear Quantum Momentum as a Hidden Agent, *Phys. Rev. Lett.* **133**, 233201 (2024).
  - [2] F. Agostini, S. K. Min, A. Abedi, and E. K. U. Gross, Quantum-Classical Nonadiabatic Dynamics: Coupled- vs Independent-Trajectory Methods, *J. Chem. Theory Comput.* **12**, 2127 (2016).
  - [3] S. K. Min, F. Agostini, and E. K. U. Gross, Coupled-Trajectory Quantum-Classical Approach to Electronic Decoherence in Nonadiabatic Processes, *Phys. Rev. Lett.* **115**, 073001 (2015).
  - [4] J.-K. Ha and S. K. Min, Independent trajectory mixed quantum-classical approaches based on the exact factorization, *J. Chem. Phys.* **156**, 174109 (2022).
  - [5] E. V. Arribas and N. T. Maitra, Energy-conserving coupled trajectory mixed quantum-classical dynamics, *J. Chem. Phys.* **158**, 161105 (2023).
  - [6] J. C. Tully, Molecular dynamics with electronic transitions, *J. Chem. Phys.* **93**, 1061 (1990).
  - [7] J.-K. Ha, I. S. Lee, and S. K. Min, Surface Hopping Dynamics beyond Nonadiabatic Couplings for Quantum Coherence, *J. Phys. Chem. Lett.* **9**, 1097 (2018).
  - [8] N. Shenvi, J. E. Subotnik, and W. Yang, Phase-corrected surface hopping: Correcting the phase evolution of the electronic wavefunction, *J. Chem. Phys.* **135**, 024101 (2011).
  - [9] M. Feit, J. Fleck, and A. Steiger, Solution of the Schrödinger equation by a spectral method, *J. Comput. Phys.* **47**, 412 (1982).
  - [10] G. Granucci and M. Persico, Critical appraisal of the fewest switches algorithm for surface hopping, *J. Chem. Phys.* **126**, 134114 (2007).
  - [11] J. Xu and L. Wang, Branching corrected surface hopping: Resetting wavefunction coefficients based on judgement of wave packet reflection, *J. Chem. Phys.* **150**, 164101 (2019).
  - [12] C. Shao, Z. Shi, J. Xu, and L. Wang, Learning decoherence time formulas for surface hopping from quantum dynamics, *J. Phys. Chem. Lett.* **14**, 7680 (2023).